

Gravitational Production of Heavy Particles during and after Inflation

Davide Racco,^{a,b,c,1} **Sarunas Verner**,^{d,2} and **Wei Xue**^{d,3}

^a*Institut für Theoretische Physik, ETH Zürich,
Wolfgang-Pauli-Str. 27, 8093 Zürich, Switzerland*

^b*Physik-Institut, Universität Zürich,
Winterthurerstrasse 190, 8057 Zürich, Switzerland*

^c*Stanford Institute for Theoretical Physics, Stanford University,
382 Via Pueblo Mall, Stanford, CA 94305, USA*

^d*Institute for Fundamental Theory, Physics Department, University of Florida,
Gainesville, FL 32611, USA*

E-mail: dracco@phys.ethz.ch, verner.s@ufl.edu, weixue@ufl.edu

ABSTRACT: We investigate the gravitational production of a scalar field χ with a mass exceeding the Hubble scale during inflation $m_\chi \gtrsim H_I$, employing both analytical and numerical approaches. We demonstrate that the steepest descent method effectively captures the epochs and yields of gravitational production in a compact and simple analytical framework. These analytical results align with the numerical solutions of the field equation. Our study covers three spacetime backgrounds: de Sitter, power-law inflation, and the Starobinsky inflation model. Within these models, we identify two distinct phases of particle production: during and after inflation. During inflation, we derive an accurate analytic expression for the particle production rate, accounting for a varying Hubble rate. After inflation, the additional burst of particle production depends on the inflaton mass around its minimum. When this mass is smaller than the Hubble scale during inflation, H_I , there is no significant extra production. However, if the inflaton mass is larger, post-inflation production becomes the dominant contribution. Furthermore, we explore the implications of gravitationally produced heavy fields for dark matter abundance, assuming their cosmological stability.

Contents

1	Introduction	1
2	Gravitational Production of a Spectator Field	4
2.1	Bogoliubov Transformation	4
2.2	Steepest Descent Method and Particle Number Density	7
3	Inflationary Models	10
3.1	de Sitter to Minkowski universe transition	10
3.2	Power-Law Inflation	13
3.3	Starobinsky Model of Inflation	16
4	Reheating and Dark Matter Abundance	21
5	Discussion and Conclusions	26
A	WKB Approximation	28
B	Stokes Line Approach	29

1 Introduction

Multiple features of the Universe that we observe on large scales point to the paradigm of primordial inflation as a framework that describes the initial conditions and early dynamics of the observable Universe (see e.g. [1–3] for reviews). Inflation marks an early stage of accelerated expansion in the universe. This rapid expansion serves as a generator of new particles, including those with minimal couplings to gravity [4–7].

These particles arise through minimal and inevitable gravitational interactions, influencing diverse phenomena, such as dark matter, cosmological (iso)curvature perturbation, baryon asymmetry, and gravitational waves (see [8] for a review). The existence of dark matter is supported by gravitational probes, but there is no evidence yet of other interactions, making the minimal gravitational production an attractive and motivated option. This mechanism has been studied for dark matter consisting of a single particle that couples only through gravity, with different evolution histories depending on its spin: 0 [9–13], $\frac{1}{2}$ [14–16], 1 [17–22], $\frac{3}{2}$ [23–26], 2 [27]. Beyond dark matter, gravitational production inevitably yields a contribution to dark sector as a byproduct of inflation, as explored in [28–36]. Furthermore, depending on the particle’s mass, spin, and interactions, the (post-)inflationary production of particles may overclose the Universe (e.g. in the case of light, weakly coupled scalar fields), produce non-Gaussianities, or excessive isocurvature fluctuations on the large scales probed by the cosmic microwave background (CMB) [37–43].

Gravitational particle creation occurs during inflation, and also after inflation. The beginning of the thermal history of the Universe during the (p)reheating phase after inflation may provide further graviton-mediated particle production via scattering of massive inflaton modes or hot Standard Model (SM) particles [44–72].

Motivated by this rich phenomenology, and by the following theoretical inquiries, we investigate the gravitational production of a heavy scalar field χ , with a mass m_χ larger than the inflationary Hubble rate H_I .

Phenomenologically, scalar masses are generally not protected by symmetries from large corrections, leading to the natural expectation that they are heavy, near the scale of new physics. When these particles are heavier than the Hubble rate during inflation, their spectrum of perturbations becomes blue-tilted (i.e. enhanced on short scales), thus avoiding problematic isocurvature perturbations on the CMB scales. Moreover, the gravitational production of heavy scalars is typically suppressed, thereby preventing overproduction and rendering them promising candidates for dark matter.

In theoretical terms, several crucial questions regarding the production of a simple spin-0 particle in an inflationary background remain unanswered. These include: 1) determining the particle production rate during inflation, accounting for the time variation of the Hubble rate; 2) understanding the model dependence of heavy particle production; 3) comprehending particle production during and after inflation within a unified framework.

Previous literature has primarily focused on particle production during inflation within de Sitter spacetime, or equivalently, by assuming a constant Hubble rate, yielding a number density $\sim \exp(-2\pi m_\chi/H_I)$ [73–75]. However, the Hubble rate during inflation undergoes gradual changes. After 60 e -foldings, this variation can result in a significant modification in the predicted particle abundance, as the Hubble rate modifies exponentially the produced number density. Additionally, the final abundance of heavy particles is predominantly influenced by the UV modes which are almost leaving the Hubble radius at the end of inflation, when the Hubble rate changes even more rapidly. Therefore, this motivates us to explore the particle production with a slow-rolling Hubble scale during inflation.

After inflation, the coherent oscillations of the inflaton field around its minimum can trigger the production of χ through gravitational interactions. Previous studies [45, 47, 51] highlighted the possibility that gravitational particle production may not be exponentially suppressed when $m_\phi > m_\chi \gg H_I$, because of graviton-mediated pair annihilations of the inflaton ϕ into the scalar field χ . Some analytic treatment was developed in [76]. A gap between the inflaton mass in its minimum, and the inflationary H_I , can be realized in the hilltop inflationary model. In our study, we focus on the complementary parameter space, where the inflaton mass is smaller than or comparable to the spectator mass, i.e. $m_\phi \lesssim m_\chi$ and $m_\chi \gtrsim H_I$. Notably, this parameter space can naturally arise in various inflationary models.

In our paper, we present a comprehensive analytical and numerical analysis of heavy particle production during and after inflation. To compute particle production rates during these phases, we employ the Wentzel-Kramers-Brillouin (WKB) approximation and the steepest descent method [77–79] to determine the Bogoliubov coefficients. Unlike the Stokes line method utilized in previous studies about gravitational production [74, 79–81], the

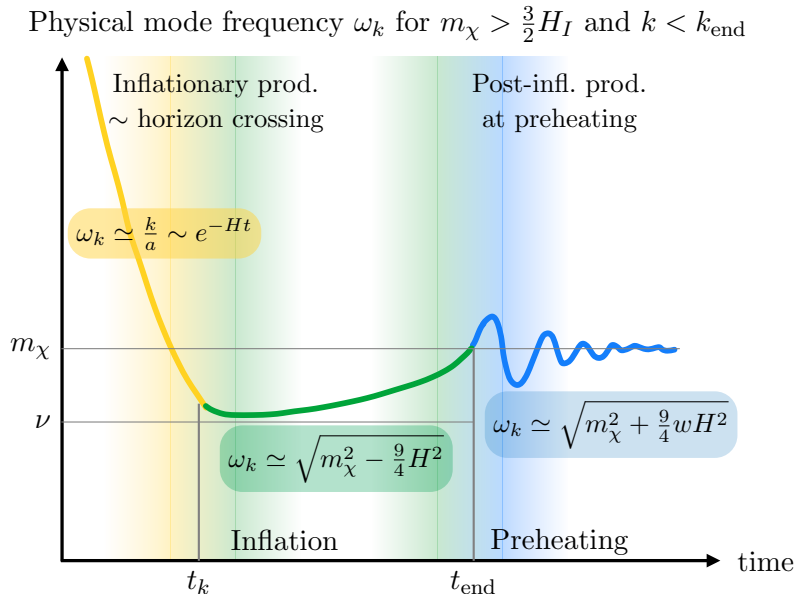


Figure 1. Evolution of the physical mode frequency ω_k defined in Eqs. (2.5) and (2.10) as a function of cosmic time t , for a massive scalar ($m_\chi > H_I$) and $k < k_{\text{end}} = a_{\text{end}}H_{\text{end}}$. The zeros (in the complex t plane) of the analytical extension of $\omega_k(t)$ determine the relevant epochs of particle production, and the saddle points (see Fig. 2) for the evaluation of the Bogoliubov coefficient β_k . Until the time t_k (fixed by $\frac{k^2}{a(t_k)^2} = m_\chi^2 - \frac{9}{4}H(t_k)^2$, just before Hubble exit), the dispersion relation is dominated by the exponentially decaying physical momentum (in yellow), while during the green epoch ω_k is almost a constant. After the end of inflation t_{end} , the $a(t)$ -dependent term oscillates as an effect of the pressure variation during the inflaton oscillations around its minimum (preheating). Particle production of the massive scalar occurs around the transition regions of Hubble crossing and preheating.

steepest descent method simplifies the treatment as it eliminates the need to compute Stokes multipliers [81]. Using the WKB approximation and steepest descent method, we can keep track of particle production around the two transition regions at the times of Hubble crossing and preheating, as illustrated in Fig. 1. For our numerical analysis, we solve the equations of motion of χ , evaluating the particle occupation number at late times. We conduct a thorough comparison of the occupation number computed with analytic and numerical approaches. Finally, we relate the produced number density to the present abundance of the scalar, to assess its viability as a dark matter candidate.

Our study encompasses three distinct inflationary scenarios. We first consider a simple de Sitter space transitioning smoothly to a flat Minkowski background, to recover previous findings of the exponentially suppressed particle production. In the second scenario, we explore the analytic model power-law inflation [82, 83] to examine particle production with a varying Hubble rate during inflation. To understand the dependence on the inflationary model, and compare the particle production occurring during and after inflation, we consider as a third scenario the Starobinsky model of inflation [84], which aligns well with current data from Planck and BICEP.

This paper is structured as follows. In Section 2, we discuss the gravitational produc-

tion of spectator scalar fields, introducing the Bogoliubov transformation and the method of steepest descent. Section 3 examines three specific inflationary scenarios: the transition from a de Sitter phase to a flat Minkowski universe, power-law inflation, and the Starobinsky model of inflation. We compute the dark matter abundance for these models in Section 4. Our conclusions are presented in Section 5. Additionally, a detailed discussion of the higher-order WKB approximation and a comparison between the steepest descent method and the Stokes line approach are provided in Appendix A and in Appendix B.

2 Gravitational Production of a Spectator Field

In this section, we establish the foundation for evaluating the particle number density resulting from gravitational production. The production rate is determined by solving the field equations and employing WKB approximation. We then compute the particle occupation number at the late time of the universe using the Bogoliubov transformation approach, with the Bogoliubov coefficients derived through the steepest descent approach.

2.1 Bogoliubov Transformation

To compute particle production in curved spacetime, we employ the Bogoliubov transformation approach [5, 85, 86]. This method allows us to describe the adiabatic evolution of the produced particle wave function, taking into account the effects of curved spacetime. The evolution results in a mixture of positive and negative frequency modes, which characterizes the particles generated by the expansion of spacetime.

We begin our discussion by considering a background geometry that is homogeneous and isotropic, and can be effectively modeled using the Friedmann-Robertson-Walker (FRW) spacetime metric:

$$ds^2 = g_{\mu\nu} dx^\mu dx^\nu = dt^2 - a(t)^2 d\mathbf{x}^2, \quad (2.1)$$

where t represents cosmic time, $a(t)$ is the dimensionless scale factor, and \mathbf{x} denotes the 3-dimensional comoving spatial vector. Throughout this paper, we focus on cosmic rather than conformal time.

We introduce a spectator scalar field, χ , with an action given by

$$\mathcal{S}_\chi = \int d^4x \sqrt{-g} \left(\frac{1}{2} g^{\mu\nu} \partial_\mu \chi \partial_\nu \chi - \frac{1}{2} m_\chi^2 \chi^2 \right). \quad (2.2)$$

The kinetic term of the field is canonically normalised by introducing a rescaled field X ,¹

$$X(t, \mathbf{x}) \equiv a(t)^{\frac{3}{2}} \chi(t, \mathbf{x}). \quad (2.3)$$

With this redefinition, the above action is modified in

$$\mathcal{S}_X = \int d^4x \mathcal{L}_X = \int d^4x \left(\frac{1}{2} g^{\mu\nu} \partial_\mu X(t, \mathbf{x}) \partial_\nu X(t, \mathbf{x}) - \frac{1}{2} H^2(t) \nu^2(t) X^2(t, \mathbf{x}) \right), \quad (2.4)$$

¹Note that rescaling the scalar field introduces ambiguity in determining particle production density via the Bogoliubov method, as it may incorporate local contributions to the energy density. This ambiguity can be resolved by measuring the particle number in (or near) flat spacetime.

where $H = \dot{a}/a$ is the Hubble rate, and we define the dimensionless variable,

$$\nu^2 = \frac{m_\chi^2}{H^2} - \frac{9}{4} - \frac{3}{2} \frac{\dot{H}}{H^2} = \frac{m_\chi^2}{H^2} + \frac{9}{4} w, \quad (2.5)$$

where $w(t) = p(t)/\rho(t)$ is the equation of state of the Universe. The field X can be expressed in Fourier space as

$$X(t, \mathbf{x}) = \int \frac{d^3\mathbf{k}}{(2\pi)^3} \left[\hat{a}_{\mathbf{k}} X_k(t) e^{i\mathbf{k}\cdot\mathbf{x}} + \hat{a}_{\mathbf{k}}^\dagger X_k^*(t) e^{-i\mathbf{k}\cdot\mathbf{x}} \right]. \quad (2.6)$$

Here \mathbf{k} denotes the comoving momentum vector, and $\hat{a}_{\mathbf{k}}^\dagger$ and $\hat{a}_{\mathbf{k}}$ are the creation and annihilation operators, respectively, that satisfy the commutation relations $[\hat{a}_{\mathbf{k}}, \hat{a}_{\mathbf{k}'}] = [\hat{a}_{\mathbf{k}}^\dagger, \hat{a}_{\mathbf{k}'}^\dagger] = 0$ and $[\hat{a}_{\mathbf{k}}, \hat{a}_{\mathbf{k}'}^\dagger] = (2\pi)^3 \delta^3(\mathbf{k} - \mathbf{k}')$. From the action given in Eq. (2.4), we derive the conjugate momentum of X , given by $\pi \equiv \partial\mathcal{L}_X/\partial\dot{X} = \dot{X}$. To quantize the system, we impose the commutation relation

$$[X(t, \mathbf{x}), \pi(t, \mathbf{y})] = i\delta^3(\mathbf{x} - \mathbf{y}), \quad (2.7)$$

which, along with the commutation relations of the creation and annihilation operators, implies the Wronskian condition:

$$X_k \dot{X}_k^* - X_k^* \dot{X}_k = i. \quad (2.8)$$

The field equation for X in Fourier space, as a consequence of the rescaling in Eq. (2.3), does not display a term of Hubble friction, and is given by

$$\ddot{X}_k(t) + \omega_k^2(t) X_k(t) = 0, \quad (2.9)$$

with

$$\omega_k^2 = \frac{k^2}{a^2} + H^2 \nu^2. \quad (2.10)$$

Next, applying the *adiabatic* (WKB) approximation, we assume that the wave function $X_k(t)$ can be expressed as the sum of its solutions $\exp(\pm i \int \omega_k dt)$ [86]

$$X_k(t) = \frac{\alpha_k}{\sqrt{2\omega_k}} e^{-i \int^t \omega_k dt} + \frac{\beta_k}{\sqrt{2\omega_k}} e^{+i \int^t \omega_k dt}, \quad (2.11)$$

where α_k and β_k are the time-dependent Bogoliubov coefficients.

The adiabatic approximation is exact in the limit in which the wave function evolves adiabatically and satisfies the condition $|\dot{\omega}_k| \ll |\omega_k|^2$ at all times during the evolution. In Eq. (2.11), ω_k corresponds to the zeroth-order of the WKB expansion, while high-order frequency will be implemented in the numerical analysis to achieve a faster convergence of the results to the actual solution. The frequency for the j -th order improved WKB approximation is given by the iterative formula,

$$\omega_k^{(j)} = \sqrt{\omega_k^2 - \left[\frac{\ddot{\omega}_k^{(j-1)}}{2\omega_k^{(j-1)}} - \frac{3}{4} \left(\frac{\dot{\omega}_k^{(j-1)}}{\omega_k^{(j-1)}} \right)^2 \right]}, \quad (2.12)$$

starting with $\omega_k^{(0)} = \omega_k$. Further discussion on the high-order WKB approximation is provided in Appendix A.

The time-dependent Bogoliubov coefficients are correlated via the field equations Eq. (2.9), leading to the following relationships:

$$\dot{\alpha}_k(t) = \frac{\dot{\omega}_k}{2\omega_k} \beta_k e^{2i \int^t \omega_k dt}, \quad \dot{\beta}_k(t) = \frac{\dot{\omega}_k}{2\omega_k} \alpha_k e^{-2i \int^t \omega_k dt}. \quad (2.13)$$

By combining these equations with the Wronskian condition in Eq. (2.8), we find the normalization condition for the Bogoliubov coefficients:

$$|\alpha_k|^2 - |\beta_k|^2 = 1. \quad (2.14)$$

To solve the mode equation (2.9), we must impose the initial conditions. Using the WKB approximation in the early-time limit, $t \rightarrow -\infty$, we choose the well-known Bunch-Davies conditions for the initial vacuum state:

$$\lim_{t_i \rightarrow -\infty} X_k(t_i) = \frac{1}{\sqrt{2\omega_k(t_i)}} e^{-i \int^{t_i} \omega_k dt}. \quad (2.15)$$

Comparing this to the adiabatic form of the wave function in Eq. (2.11), one sees that

$$\alpha_k(t_i) = 1, \quad \beta_k(t_i) = 0, \quad (2.16)$$

where t_i is an initial time satisfying the Bunch-Davies vacuum conditions.

The average energy density of the spectator field at any given time, $\langle H(t) \rangle$, is evaluated as

$$\langle H(t) \rangle = \left\langle \Omega \left| \int d^3 \mathbf{x} \left(\pi(t, \mathbf{x}) X(t, \mathbf{x}) - \mathcal{L}_X \right) \right| \Omega \right\rangle = \int \frac{d^3 \mathbf{k}}{(2\pi)^3} \frac{1}{2} \left(|\dot{X}_k|^2 + \omega_k^2 |X_k|^2 \right). \quad (2.17)$$

We define the dimensionless occupation number n_k as the energy density for a mode k divided by the frequency:

$$n_k(t) = \frac{1}{\omega_k} \left(\frac{1}{2} |\dot{X}_k(t)|^2 + \frac{1}{2} \omega_k^2 |X_k(t)|^2 \right) - \frac{1}{2} = \frac{1}{2\omega_k} \left| \dot{X}_k + i\omega_k X_k \right|^2 \simeq |\beta_k|^2, \quad (2.18)$$

where the leading vacuum energy contribution $-\frac{1}{2}$ is removed. The second equality in Eq. (2.18) is derived using the Wronskian condition, and the approximate equality is validated by employing the WKB approximation in Eq. (2.11). It is important to note that the normal-ordering subtraction of $\frac{1}{2}$ in Eq. (2.18) does not eliminate all local contributions to the energy density. The previous definition may leave an ambiguity in the particle occupation number at late times. However, if the inflationary background is connected to a Minkowski or matter-dominated universe, $n_k(t)$ corresponds to the occupation number of produced particles as $t \rightarrow \infty$, since the geometric contribution will be subdominant compared to the particle energy density. In numerical approaches, this quantity is computed at sufficiently late times.

In the numerical results shown in the paper, we solve for $X_k(t)$ using Eq. (2.9), and compute n_k by replacing ω_k in Eq. (2.18) with the higher-order WKB approximation

$\omega_k^{(j)}$. The occupation number n_k carries a small dependence on the order (j), stemming from the ambiguity of the vacuum states in curved spacetime or from additional vacuum contributions that necessitate subtraction. These differences vanish when evaluating the expression for n_k in Minkowski spacetime, or at asymptotically late times $t_{\text{final}} \gg t_{\text{end}}$, so that the particle occupation number becomes independent of the order of the WKB approximation. See Refs. [87, 88] for a detailed discussion.

The physical number density is obtained by integrating the occupation number n_k ,

$$n_\chi = \frac{1}{2\pi^2 a(t)^3} \int_0^\infty dk k^2 |\beta_k|^2. \quad (2.19)$$

Gravitational particle production in the regime $|\beta_k|^2 \ll 1$, $|\alpha_k| \simeq 1$, leads to [86]

$$\beta_k(t) \simeq \frac{1}{2} \int_{t_i}^t dt' \frac{\dot{\omega}_k}{\omega_k} \exp\left(-2i\Omega_k(t')\right), \quad \Omega_k(t) \equiv \int_{t_i}^t dt' \omega_k(t'). \quad (2.20)$$

We now explore analytical methods to estimate this solution for β_k .

2.2 Steepest Descent Method and Particle Number Density

After having introduced the Bogoliubov transformation to derive the occupation number in Eq. (2.20), we proceed to evaluate the integral using the steepest descent method, paralleling the methodology outlined in [77–79].

The steepest descent method shows that the dominant contribution to the integral in Eq. (2.20) arises from the region near the saddle points in the complex t plane. We deform the integration contour for β_k so that it passes through these saddle points along the appropriate directions, where the real part of the exponential term in the integrand decreases most rapidly and the imaginary part is constant (hence the alternative name of “constant phase”). This guarantees that the integrand decreases quickly as one moves away from the saddle point.

The first step is to identify the saddle points for the integral in Eq. (2.20). They are determined by setting the derivative of the exponent to zero, $\frac{d}{dt}\Omega(t) = 0$, which leads to

$$\omega_k(t_n) = 0. \quad (2.21)$$

These saddle points for the integral of β_k happen to coincide with the *poles* of the integrand, and we often refer to them as n -th pole.

Starting from the squared mode frequency in Eq. (2.10), we expand $\omega_k^2(t)$ near the n -th saddle point to find the steepest descent paths,

$$\Omega_k(t) \simeq \int_{t_i}^{t_n} dt' \omega_k(t') + \sqrt{g(t_n)} \int_{t_n}^t dt' \sqrt{(t' - t_n)} = \int_{t_i}^{t_n} dt' \omega_k(t') + \frac{2}{3} \sqrt{g(t_n)} (t - t_n)^{3/2}, \quad (2.22)$$

where

$$g(t_n) \equiv \left. \frac{d}{dt} \omega_k^2(t) \right|_{t=t_n}. \quad (2.23)$$

Integration contour for β_k in the steepest descent approximation

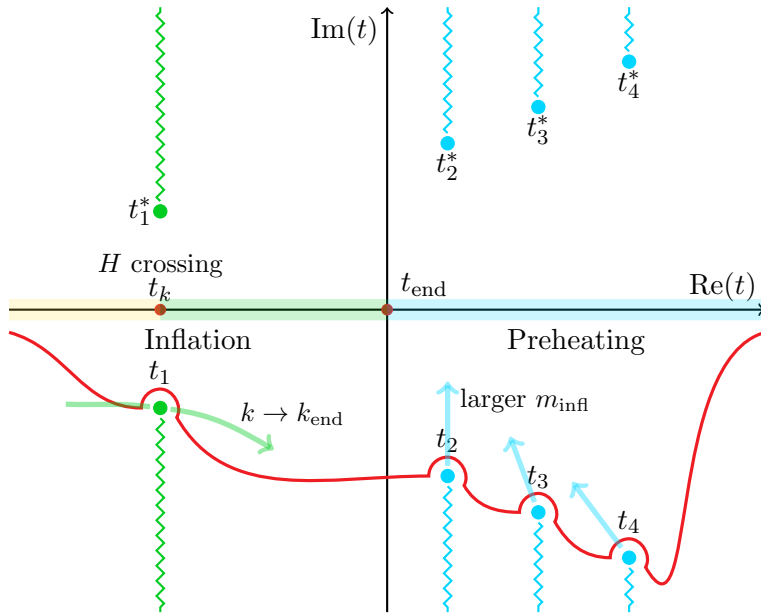


Figure 2. The integration path for β_k on the complex t plane. The colour shadings on the real axis reflect the colour code of Fig. 1 about the sub-Hubble, super-Hubble and post-inflationary epochs for the mode frequency $\omega_k(t)$. The saddle points t_n (given by $\omega_k(t_n) = 0$) of the integrand of β_k are indicated by dots, and the branch cuts are shown with zigzag lines. The red line is the contour for the saddle-point approximation of β_k , whose path around the poles covers an angle $4\pi/3$ avoiding the branch cut. From a quantitative point of view, the most relevant saddle point for the computation of β_k is the closest one to the real t axis. The green and blue arrows show the displacement of the saddle points as we vary k and the inflaton mass. If we increase the spectator field mass m_χ , all saddle points get further away from the real axis, suppressing exponentially the particle production.

Notice that the square root in Eq. (2.22) introduces branch cuts originating from the saddle points t_n . With this expansion we approximate the prefactor in Eq. (2.20) as

$$\frac{\dot{\omega}_k(t)}{2\omega_k(t)} \simeq \frac{1}{4} \frac{1}{t - t_n}. \quad (2.24)$$

We illustrate the steepest descent path of integration on the complex plane in Fig. 2. We deform the contour in the lower half-plane, and Eq. (2.20) transforms into a sum of the saddle point contributions

$$\beta_k \simeq \sum_n V_n \exp \left[-2i \int_{t_i}^{t_n} dt' \omega_k(t') \right] \quad (2.25)$$

$$V_n = \frac{1}{4} \int_{C_n} \frac{dt}{t - t_n} \exp \left[-\frac{4i}{3} \sqrt{g(t_n)} (t - t_n)^{3/2} \right]. \quad (2.26)$$

We evaluate the coefficients V_n along the deformed contour C_n that approaches the n -th pole along the path of steepest descent and then goes around this pole. Importantly, this general expression accounts for contributions from all n poles (saddle points).

The constant-phase paths are selected by the phase $\arg(V_n) = (2j + 1)\pi$, $j \in \mathbb{Z}$. Denoting $\theta \equiv \arg(t - t_n)$, $\varphi \equiv \arg(g(t_n))$,

$$\frac{3\pi}{2} + \frac{\varphi}{2} + \frac{3\theta}{2} = (2j + 1)\pi \Rightarrow \theta = \frac{(4j - 1)\pi - \varphi}{3}, \quad (2.27)$$

For the dispersion relation of Eq. (2.10) and the supermassive case $m_\chi > \frac{3}{2}H_I$ that we consider, $\varphi = 0$ for all saddle points. Regarding the branch cuts introduced in each saddle point by the square root of Eq. (2.22), we choose to align them with vertical lines to $\pm i\infty$ as shown in Fig. 2. The contour C_n can then avoid the branch cut by picking $j = 1$ as ingoing phase ($\theta = \pi$) and $j = 0$ as outgoing phase ($\theta = -\frac{\pi}{3}$), as shown in Fig. 2. Consequently, by evaluating the prefactor along the contour C_n in the limit of vanishing radius, we obtain

$$V_n \simeq \frac{1}{4} \times \frac{4\pi}{3} i = \frac{i\pi}{3}. \quad (2.28)$$

Next, we evaluate the exponent $\Omega_k(t)$ in Eq. (2.25). The contour of integration for Ω_k can be freely modified, as $\omega_k(t)$ is an analytic function. It is important to note that the integration path of Eq. (2.25) does not need to coincide with the contour for β_k . We split the integral as

$$\int_{t_i}^{t_n} dt' \omega_k(t') = \int_{t_i}^{\text{Re } t_n} dt' \omega_k(t') + \int_{\text{Re } t_n}^{t_n} dt' \omega_k(t'). \quad (2.29)$$

The first term in Eq. (2.29) is real, contributing as a phase to each pole's contribution. This term cancels when considering the contribution from a single pole, though it may have a small effect when summing multiple poles, even if the integral along the real axis typically contributes less. Therefore, the occupation number for the mode k takes the form

$$|\beta_k|^2 \simeq \frac{\pi^2}{9} \left| \sum_n e^{2\text{Im } \Omega_k(t_n)} \right|^2 \simeq \frac{\pi^2}{9} \left| \sum_n \exp \left(-2i \int_{\text{Re } t_n}^{t_n} dt' \omega_k(t') \right) \right|^2. \quad (2.30)$$

We use this equation to compute the particle number both analytically and numerically in Section 3. The particular contour for $\Omega_k(t)$ in Eq. (2.29) is utilized for the models of de Sitter and Starobinsky inflation, while different paths are chosen for power-law inflation to obtain an analytic formula.

The result can further be approximated by noting that $\omega_k(t)$ has an almost constant modulus for most of the path from $\text{Re}(t_n)$ to t_n . Within that approximation,

$$\int_{t_i}^{t_n} dt' \omega_k(t') \simeq i \text{Im} \left(\int_{\text{Re } t_n}^{t_n} dt' \omega_k(t') \right) \simeq i \omega_k(\text{Re}(t_n)) \times \text{Im}(t_n), \quad (2.31)$$

and the occupation number of produced particles becomes

$$|\beta_k|^2 \simeq \frac{\pi^2}{9} \left| \sum_n e^{2\omega_k(\text{Re}(t_n)) \times \text{Im}(t_n)} \right|^2. \quad (2.32)$$

This result provides a good analytical estimate.

Alternatively, Stokes's method can be employed for the integration. The comparison between the steepest descent method and Stokes's method is detailed in Appendix B.

3 Inflationary Models

In this section, we explore the model dependence of gravitational particle production, examining its occurrence during and after inflation within a unified framework. Our examination encompasses three distinct scenarios: de Sitter spacetime, power-law inflation, and the Starobinsky model of inflation. To ensure a comprehensive analysis and comparison, we apply both the numerical solution and the analytical steepest descent approach to each scenario.

3.1 de Sitter to Minkowski universe transition

We explore a simple scenario where de Sitter spacetime smoothly transitions into Minkowski spacetime, characterized by the scale factor,

$$a(t) = 2a_{\text{end}} \frac{e^{H_I(t-t_{\text{end}})}}{1 + e^{H_I(t-t_{\text{end}})}}. \quad (3.1)$$

Here, H_I represents a constant Hubble parameter during the de Sitter phase and t_{end} marks the transition time from de Sitter to flat spacetime. This schematic cosmological evolution simplifies the calculation of the gravitationally produced abundance because it displays a quick transition to an asymptotically flat spacetime.

The following discussion includes the gravitational particle production of a heavy scalar field, analyzed using two complementary approaches: the numerical solution of the scalar field evolution in the spacetime background and the approximate WKB approach. Fig. 3 shows the consistency of the two methods.

Numerical approach

We first determine the plane-wave solutions of the scalar field numerically by solving the field equation $\ddot{X}_k + \omega_k^2(t)X_k = 0$, with

$$\omega_k^2 = \frac{k^2}{a^2} + H_I^2 \nu^2 = \frac{k^2(1 + e^{H_I(t-t_{\text{end}})})^2}{4a_{\text{end}}^2 e^{2H_I(t-t_{\text{end}})}} + m^2 + \frac{3(-3 + 2e^{H_I(t-t_{\text{end}})})}{4(1 + e^{H_I(t-t_{\text{end}})})^2} H_I^2. \quad (3.2)$$

The expression for ω_k^2 in the specific spacetime background is detailed in the equation. The initial condition is set at a sufficiently early time using the WKB approximation, as expressed in Eq. (2.15). We then solve the field equation for $X_k(t)$ with the initial condition. Following this, the occupation number n_k at a given time t (2.18) is evaluated using the mode frequency for the j -th order improved WKB approximation shown in Eq. (2.12). In Fig. 3, we use the first-order improved WKB approximation for a better numerical precision. The particle occupation number $n_k = |\beta_k|^2$ is presented as a function of t in units of H_I^{-1} (top panels) for two distinct mass choices $m_\chi = 2H_I$ (left panels) and $m_\chi = 3H_I$ (right panels). The time evolution of n_k reveals an initial increase followed by a subsequent decrease. This behavior is not physical and changes if we use a different order of WKB approximation: the physical quantity is the asymptotic value reached at late times. From a numerical perspective, the absolute accuracy in tracking the exponentially suppressed occupation number n_k is set by the initial value of the mode function $|X_k(t_i)| =$

de Sitter inflation to Minkowski

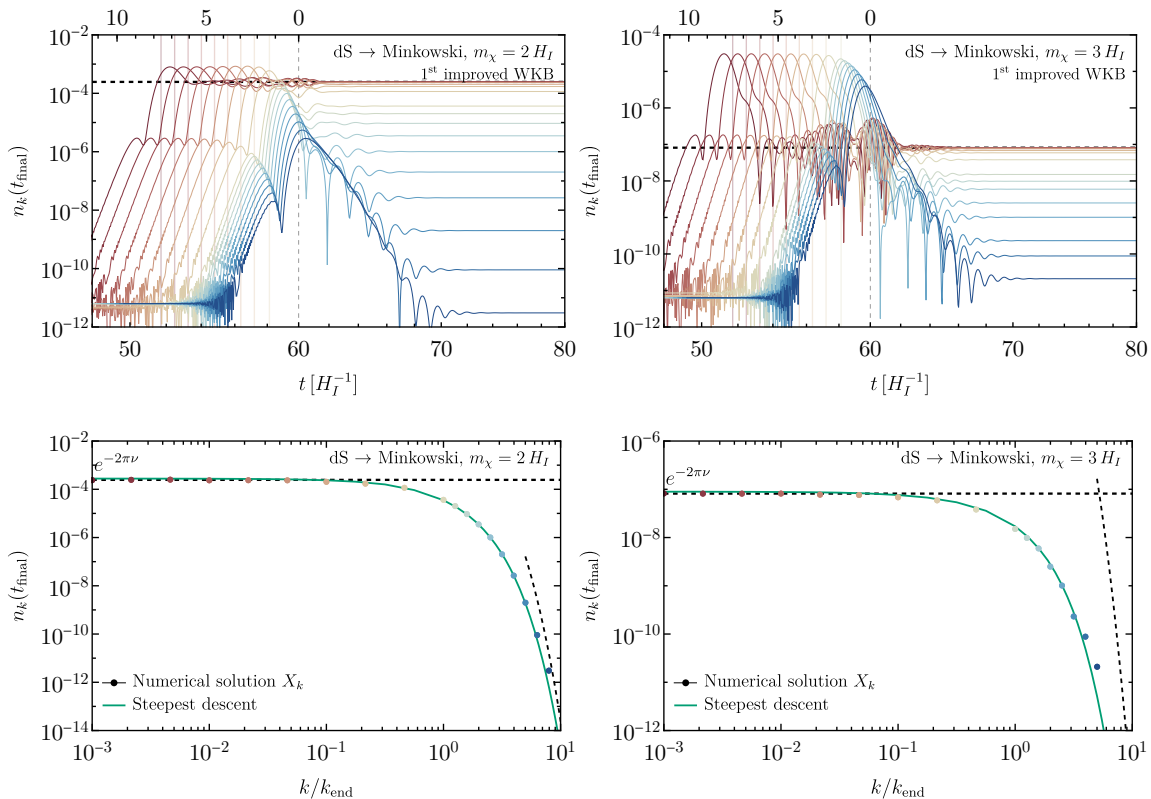


Figure 3. Particle occupation number $n_k = |\beta_k|^2$ as a function of time t in H_I^{-1} units (top panels) and of momentum k/k_{end} (bottom panels, where n_k is evaluated at a late time t_{final}) for two representative mass choices of $m_\chi = 2H_I$ (left panels) and $m_\chi = 3H_I$ (right panels). Each colored line in the top plots corresponds to the momentum marked in the bottom plots by a point with the same color. The color grading from red to blue reflects the transition from IR ($k < k_{\text{end}}$) to UV modes ($k > k_{\text{end}}$). In the bottom plots, the green line is the result of the steepest descent method where the saddle points and the integral of Eq. (2.30) are evaluated numerically. The black dashed lines show the analytical approximations of the steepest descent method computed in this section. The steepest descent approximation is in excellent agreement with the fully numerical computation.

$1/\sqrt{2\omega_k(t_i)} \simeq \sqrt{a(t_i)/k}$. Pushing t_i to earlier times (especially at small k) increases the numerical precision of n_k , which can be read off in our results from the (unphysical) plateau at early times in the top panels of Figs. 3, 4, 6, 7.

The final spectra for the occupation number n_k are evaluated at a late time $t_{\text{final}} = 200 H_I^{-1} \gg t_{\text{end}}$ (we compute a time average of the small residual oscillations), and are shown in the bottom panel of Fig. 3 as a function of the rescaled momentum k/k_{end} , where $k_{\text{end}} \equiv a_{\text{end}} H_I$ is the mode crossing the Hubble radius at the end of inflation.

The spectrum n_k comprises a UV ($k \gg k_{\text{end}}$) and an IR part ($k \ll k_{\text{end}}$). The long wavelength (IR) spectrum is flat in k , as shown in Fig. 3, consistent with known results for particle production in de Sitter for heavy scalar fields. The IR spectrum is $n_k \sim \exp(-2\pi\nu)$

with $\nu \equiv \sqrt{m^2/H_I^2 - 9/4}$, marked by horizontal dashed lines in the bottom panels of Fig. 3. This occupation number, in the limit $m_\chi \gg H_I$, is analogous to the Bose-Einstein distribution for a heavy particle at a Gibbons-Hawking temperature $T_{\text{dS}} = H_I/2\pi \ll m_\chi$.

The short wavelength (UV) spectrum is exponentially suppressed with respect to k . These modes never left the Hubble radius during inflation. From the numerical perspective of the equations of motion for X_k , the non-adiabaticity parameter $\dot{\omega}_k/\omega_k^2$ is suppressed by the large $\omega_k \sim k/a$ during inflation, reducing the gravitational production for these modes.

Analytical approach

We now compare the numerical results obtained by solving the equations of motion for X_k , with the analytical formula for β_k obtained with the steepest descent approximation, as detailed in Section 2.2. We first consider the IR modes, for which particle production occurs before the end of inflation. In this first model where the inflationary epoch is almost exactly de Sitter, the Hubble rate is a constant H_I . The saddle points t_n are easily obtained in this case by solving $\omega_k(t_p) = 0$ with constant H_I and ν :

$$H_I(t_n - t_{\text{end}}) = \log\left(\frac{k}{a_{\text{end}}H_I\nu}\right) - i\frac{\pi}{2} - in\pi, \quad n \in \mathbb{Z}. \quad (3.3)$$

The dominant saddle point in the lower half-plane is at $n = 0$, since it is closest to the real t axis and minimizes the exponential suppression in Eq. (2.20). That formula, for the case of one saddle point, simplifies into

$$n_k \simeq |\beta_k|^2 \simeq \frac{\pi^2}{9} \exp\left(-2i \int_{t_p^*}^{t_p} dt \omega_k(t)\right). \quad (3.4)$$

The exponent of this expression, for the pole of Eq. (3.3), is equal to

$$-2i \int_{t_p^*}^{t_p} dt \omega_k(t) = -2i\nu \int_{\frac{\pi}{2}i}^{-\frac{\pi}{2}i} d(H_I t) \sqrt{e^{-2H_I t} + 1} = -2\pi\nu. \quad (3.5)$$

The occupation number for IR modes is then

$$n_k^{(\text{IR})} \simeq \frac{\pi^2}{9} e^{-2\pi\nu}. \quad (3.6)$$

This result agrees with alternative methods, such as the in-out formalism [73, 89, 90] and the Stokes line method [74, 75].

Short wavelength modes $k \gg k_{\text{end}}$ never cross the Hubble radius during inflation. Particle production for UV modes hence occurs at t_{end} when the spacetime transitions into Minkowski. By considering Fig. 1, the green band of $\omega_k \sim H_I\nu$ disappears, and the yellow band where $\omega_k \sim ke^{H_I(t_{\text{end}}-t)}/a_{\text{end}}$ directly connects to the post-inflationary phase (shaded in blue). When solving $\omega_k(t_n) = 0$ for the saddle points in the limit $k \gg k_{\text{end}}$ limit, from Eq. (3.2) at 0th order in $\frac{k}{k_{\text{end}}}$ we see that $1 + e^{H_I(t-t_{\text{end}})}$ must be very close to 0, so that the gradient term in Eq. (3.2) is sufficiently small that the overall expression for ω_k^2 can

vanish. As a result, the poles are around $t_p \sim t_{\text{end}} + i\pi H_I^{-1}(2n+1)$, $n \in \mathbb{Z}$. Solving $\omega_k = 0$ around $t_{\text{end}} - i\pi H_I^{-1}$ in the limit $k \gg k_{\text{end}}$, yields four roots,

$$e^{H_I(t-t_{\text{end}})} = -1 + e^{i\frac{\pi}{2}n}(60)^{1/4} \sqrt{\frac{k_{\text{end}}}{k}} + \mathcal{O}\left(\frac{k_{\text{end}}}{k}\right), \quad n = 0, 1, 2, 3 \quad (3.7)$$

By accounting for the contribution from the pole closer to the real t axis, and assuming that a single saddle point dominates the integral for β_k , we find the occupation number for UV modes

$$n_k^{(\text{UV})} \simeq \frac{\pi^2}{9} e^{-2\pi \frac{k}{k_{\text{end}}}}. \quad (3.8)$$

We can see from Fig. 3 that the agreement of this approximate formula with numerical results is good for $k > (5-10)k_{\text{end}}$.

This agreement with numerical findings highlights the effectiveness of the steepest descent approach. From a computational point of view, the steepest descent approximation is extremely fast and sets no limits on the value of m_χ/H_I that can be used for the computation. On the contrary, the numerical solution for the mode X_k is computational intensive, and the required precision gets quickly unattainable as we increase the particle mass and the exponential suppression on its abundance. For these reasons, we rely on the steepest descent approximation to extend the analysis to larger masses when computing the dark matter density and abundance. We discuss this in detail in Section 4.

3.2 Power-Law Inflation

As a second scenario, we explore the power-law inflation model [82, 83, 91], which features a scale factor slowly evolving as a power-law, and eventually transitioning to a matter-dominated universe. Despite being excluded by *Planck* constraints², this analytical model serves as an excellent test-bed for comprehending the gravitational production of particles with a varying Hubble parameter.

The motivation to delve into the power-law inflation model is twofold. First, unlike de Sitter spacetime with a constant Hubble rate, the model exhibits a slowly change in the Hubble scale. This prompts a natural question about the validity of the particle number density formula $\exp(-2\pi\nu)$ as the Hubble rate is evolving: at which time should we evaluate the Hubble rate in this formula? Second, differently from our previous example, the inflationary spacetime evolves into a matter-dominated universe. This is the realistic setting after the end inflation when the inflaton oscillates in its minimum. We now explore how gravitational particle production proceeds in this cosmological background.

In the inflating phase of power-law inflation, the scale factor scales follows a scaling law given by

$$a(t) \propto t^{\frac{1}{\varepsilon}}, \quad (3.9)$$

where ε is a constant. The Hubble rate evolves as

$$H(t) = \frac{1}{\varepsilon t}, \quad (3.10)$$

²Power-law inflation can potentially satisfy the current constraints by considering non-canonical scalar fields [92].

and ε is equal to the slow-roll parameter for the variation rate of the Hubble scale, $\varepsilon \equiv -\frac{\dot{H}}{H}$. Power-law inflation then has constant slow-roll parameter ε , and can be realized by an inflation potential with an exponential form,

$$V(\phi) = M^4 e^{-\sqrt{2\varepsilon} \phi/M_{\text{P}}}, \quad (3.11)$$

where M is a dimensionful constant and M_{P} is the Planck mass. However, the inflation potential is somewhat incomplete, as it requires the addition of an exit mechanism to enable the transition to a decelerating phase after inflation. To bridge the two phases, we model phenomenologically the scale factor as

$$a(t) \propto \frac{(t/t_{\text{end}})^{1/\varepsilon}}{1 + (t/t_{\text{end}})^{1/\varepsilon}/(t/t_{\text{end}})^{3/2}} \quad (3.12)$$

This ensures that the scale factor is proportional to $t^{1/\varepsilon}$ during the power-law inflation phase ($t \ll t_{\text{end}}$), and smoothly transitions into matter-domination as $t \gg t_{\text{end}}$, with $a \sim t^{3/2}$.

We assess the particle occupation number $n_k = |\beta_k|^2$ through numerical solution of X_k , and compare it with the steepest descent approximation for β_k . The summarized results are presented in Fig. 4 with the choice of parameters $\varepsilon = 0.02$, $t_{\text{end}} = 60H_I$, where we set the arbitrary time normalisation so that $H_I \equiv H_{N=8.4}$ is the Hubble rate at 8.4 e -folds before the end of inflation.³ The mode leaving the Hubble radius at the end of inflation is $k_{\text{end}} \equiv \dot{a}(t_{\text{end}}) = a_{\text{end}}H_{\text{end}}$.

Figure 4 illustrates the occupation number n_k as a function of time t in unit of H_I (top panels) and as a function of the rescaled momentum k/k_{end} (bottom panels) for two mass choices $m_\chi = 2H_I$ (left panels) and $m_\chi = 3H_I$ (right panels). Notably, long-wavelength (IR) modes display a non-flat behavior with a negative slope, while, consistently with our previous observation, short-wavelength (UV) modes exhibit a strong exponential suppression in k . Furthermore, we find consistent results between the full numerical solutions and the steepest descent approximation, that we discuss in the following.

Steepest descent method for a time-varying Hubble rate

As discussed in Section 2.2, the first step is to solve $\omega(t_p) = 0$. In the limit of small ε , and denoting $t_p = |t_p|e^{i\theta_p}$, we find

$$\omega^2(t_p) \simeq \frac{k^2}{a^2(|t_p|)} e^{-2i\theta_p/\varepsilon} + m_\chi^2 - \frac{9}{4}H^2(|t_p|)e^{-2i\theta_p}. \quad (3.13)$$

There are infinite saddle points with a similar real part, and separated by $2\pi i$. The saddle point t_k lying closer to the real t axis in the lower half-plane, which contributes the most to β_k , has modulus and argument given by

$$\frac{k^2}{a^2(|t_k|)} = m_\chi^2 - \frac{9}{4}H^2(|t_k|), \quad \theta_k \simeq -\frac{\pi}{2}\varepsilon, \quad (3.14)$$

³The Hubble rate in power-law inflation is $H = \frac{1}{\varepsilon t}$, and the cosmic time in our computation has units H^{-1} , where $H = 1$ at a time $t = 1/\varepsilon = 50$. At that time, 8.4 e -folds are left to reach 60 e -folds of inflation.

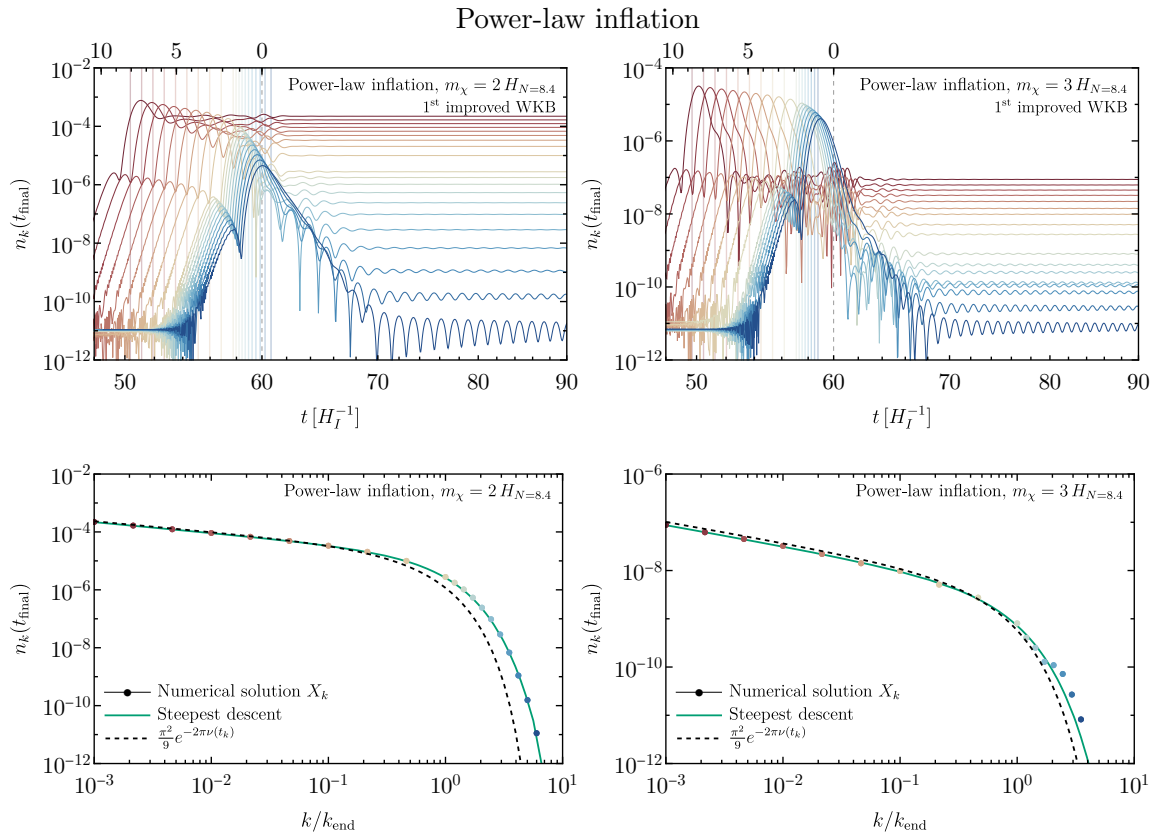


Figure 4. Same as Fig. 3 for the power-law inflation model. Here, we fix the units of m_χ/H_I to the time at 8.4 e -folds before the end of inflation. For the top panels, the upper horizontal axis marks the number of e -folds until the end of inflation, and the vertical colored lines show the value of the time t_k (for the evaluation of $\exp(-2\pi\nu(t_k))$ in the lower panel) for each mode with the corresponding color. When accounting for the time dependence of the inflationary Hubble rate, the gravitationally produced abundance can be easily estimated via Eq. (3.16), where a constant ν is replaced by $\nu(t_k)$, with t_k occurring slightly before Hubble crossing.

so that the first term in Eq. (3.13) has a phase close to π and cancels the second term. For $k \lesssim k_{\text{end}}$, we get $|t_k| \lesssim t_{\text{end}}$ and $\text{Im}(t_k) \simeq -\frac{\pi}{2}$, similarly to the analogous result for de Sitter in Eq. (3.3). Subsequently, we evaluate the exponent in Eq. (2.30),

$$-2i \int_{t_p^*}^{t_p} dt \omega_k(t) = -2i\nu(|t_p|) \int_{\frac{\pi}{2}i}^{-\frac{\pi}{2}i} d(i\theta/\varepsilon) \sqrt{e^{-2i\theta/\varepsilon} + 1} = -2\pi\nu(|t_p|). \quad (3.15)$$

In conclusion, similarly to the de Sitter case, the steepest descent approximation gives an occupation number for particle production during inflation

$$n_k \simeq \frac{\pi^2}{9} \exp\left(-2\pi\nu(t_k)\right), \quad t_k : \frac{k^2}{a^2(t_k)} = m_\chi^2 - \frac{9}{4}H(t_k)^2. \quad (3.16)$$

where $\nu(t)$ is evaluated at the time t_k when the physical wavelength $(k/a(t_k))^{-1}$ is a factor $\sim \mathcal{O}(m_\chi/H)$ smaller than the Hubble radius, so that the mode is still well inside the Hubble

radius. This analytic result is shown with black dashed lines in the lower panels of Fig. 4. For comparison, the green solid lines are computed by finding numerically the pole of $\omega_k(t)$, and by computing numerically $\Omega_k(t)$. Both the analytical and numerical results using the steepest descent method are consistent for IR modes ($k < k_{\text{end}}$). However, the analytic result (3.16) cannot be directly extrapolated to the UV modes, as the dispersion relation ($w \neq -1$) and the spacetime background are modified from the ones during inflation. We still show the simple analytical results (black dashed line) for the UV modes for comparison. Importantly, the numerical results (green line), obtained with the full dispersion relation, align well with the numerical solutions of X_k .

3.3 Starobinsky Model of Inflation

After exploring particle production in de Sitter and power-law inflation, we now delve into realistic inflationary models, to understand the implication for heavy-particle production. In this section, we focus on the Starobinsky Model, though our discussion broadly applies to other inflationary models.

The Starobinsky potential is defined as

$$V(\phi) = \frac{3}{4}\lambda M_{\text{P}}^4 \left(1 - e^{-\sqrt{\frac{2}{3\alpha}}\frac{\phi}{M_{\text{P}}}}\right)^2, \quad (3.17)$$

where λ and α are real parameters. Here, λ represents the scale of the inflationary potential, determining the Hubble scale H_I as $H_I \simeq \frac{1}{2}\sqrt{\lambda}M_{\text{P}}$. The potential is illustrated in Fig. 5 in units of M_{P} (left panel) and H_I (right panel), with α values of 0.5, 1, 3, and 5.

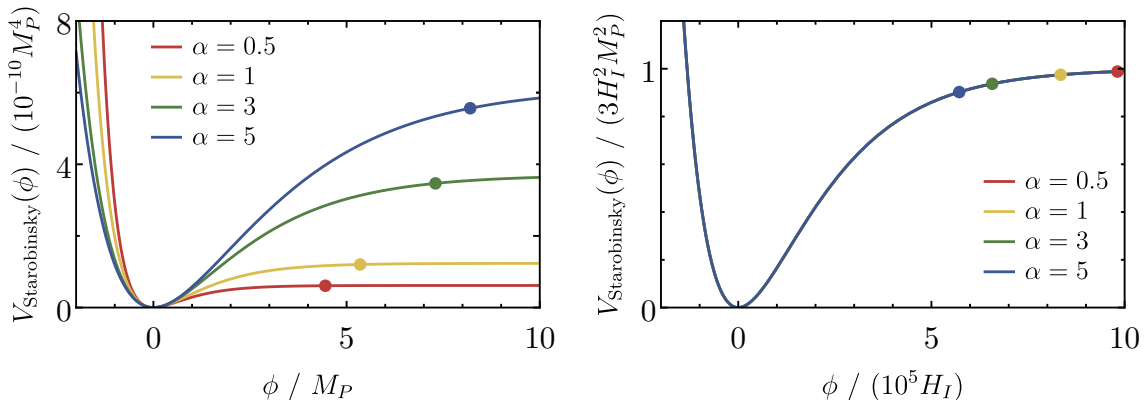


Figure 5. Starobinsky potential for different values of the parameter α . The dots mark the position of the inflaton field at $N = 60$ e -folds before the end of inflation.

To make contact with CMB observations, we can write down the predicted power spectrum \mathcal{P}_ζ , its spectral index n_s , and the tensor-to-scalar ratio r ,

$$\mathcal{P}_\zeta \simeq \frac{\lambda N_*^2}{24\pi^2 \alpha}, \quad n_s \simeq 1 - \frac{2}{N_*}, \quad r \simeq \frac{12\alpha}{N_*^2}, \quad (3.18)$$

where N_* is the number of e -folds between Hubble crossing of CMB modes and the end of inflation t_{end} .

The Hubble rate and the inflaton mass at the end of inflation are the crucial parameters governing the particle production rate. The Hubble rate slowly evolves over time, starting from a value $H_I \simeq \frac{1}{2}\sqrt{\lambda}M_{\text{P}}$ near the top of the potential. The inflaton mass after the end of inflation, when the inflation crosses the potential minimum $\phi \simeq 0$, is given by

$$m_\phi = \sqrt{\frac{\lambda}{\alpha}}M_{\text{P}} \simeq \frac{2}{\sqrt{\alpha}}H_I. \quad (3.19)$$

Thus, by utilizing CMB observations to determine the scalar power spectrum and spectral index in Eq. (3.18), we fix λ/α and therefore the inflaton mass m_ϕ , while the Hubble rate $H_I \simeq \frac{1}{2}\sqrt{\lambda}M_{\text{P}}$ varies with λ (as visible from the left panel of Fig. 5). Alternatively, when using H_I as a reference unit, variations of α correspond to a change of m_ϕ/H_I . In the following discussion, we interchangeably refer to variations of α or m_ϕ/H_I , as encoded in Eq. (3.19).

First, we present the analytic estimation for particle production after inflation. Then, on the basis of the analytic results on particle production during and after inflation, we consider two cases: light and heavy inflaton masses, with particle production occurring predominantly during and after inflation, respectively.

Analytic estimate of particle production after inflation

In the previous section, we obtained analytic results for particle production *during* inflation, with the corresponding occupation number given by Eq. (3.16). Here, we extend our analysis to estimate, the particle production after inflation, when the inflaton oscillates around the minimum of the potential, with the steepest descent approach. This method employs the analytic continuation of the frequency $\omega_k(t)$, which relies on the analytic extension of the scale factor $a(t)$. However, the exact form of $a(t)$ is inaccessible in the Starobinsky model (or any realistic inflationary model). For this reason, our analytic result within the steepest descent approach for particle production after inflation serve as an estimate, yet it remains an essential method to understand the fundamental physics. We compute an accurate occupation number through the numerical solution for the mode function X_k .

Particle production after inflation is primarily dominated by the first few oscillations of the inflaton ϕ (see e.g. [93] for the corresponding production of light fields). When oscillating around the minimum, its energy density redshifts as a non-relativistic species, so the envelope of the oscillating ϕ goes as $a^{-3/2} \sim 1/t$. Because of this redshifting amplitude, the total inflaton energy density (and hence $H(t)$) does not scale smoothly with time, and it features wiggles (although it is monotonically decreasing) of relative size $\sim H^2(t)/m_\phi^2$. An alternative description is that the equation of state $w(t)$ oscillates between the values for kination and vacuum energy, accordingly with the inflaton oscillations. This oscillating pressure induces wiggles in the frequency $\omega_k(t)$ of the superheavy field χ , as shown in Fig. 1.

For the sake of providing a simple analytical formula capturing the main parametric scaling of particle production in this epoch, we use the steepest descent approximation

with a simplified parametrisation of the inflaton by neglecting its redshift,

$$\phi(t) \simeq -\phi_0 \cos(m_\phi t), \quad (3.20)$$

where $t = 0$ marks the first time the inflaton crosses the potential minimum. For this simple estimate, we neglect the expansion of the universe within one period of the oscillation, but we take it into account for our numerical results. In the present derivation, this approximation is motivated because the first oscillation contributes most significantly to particle production due to a large value of ϕ_0 , and thus of $\sim H^2(t)/m_\phi^2$. We can then write the squared frequency of the heavy scalar χ for modes $k < k_{\text{end}}$ as

$$\omega_k^2(t) \simeq m_\chi^2 + \frac{9}{4}wH^2 \simeq m_\chi^2 + \frac{3(\dot{\phi}^2 - m_\phi^2\phi^2)}{8M_{\text{P}}^2} \simeq m_\chi^2 - \frac{9}{8}H_{\text{end}}^2 \cos(2m_\phi t), \quad (3.21)$$

where in the last step we used $3H_{\text{end}}^2 M_{\text{P}}^2 \simeq m_\phi^2 \phi_0^2$. By analytically extending ω_k to complex t , we find the closest saddle point to the real axis as

$$t_p \simeq 0 + i \frac{1}{2m_\phi} \log\left(\frac{16}{9} \frac{m_\chi^2}{H_{\text{end}}^2}\right). \quad (3.22)$$

The real part of t_p corresponds to when the inflaton crosses its potential minimum, which marks with the peak of particle production. We can then estimate the particle occupation number produced after inflation with the steepest descent approximation,

$$n_k \simeq \frac{\pi^2}{9} \exp\left(-4 \int_0^{t_p} dt \omega_k(t)\right) \simeq \frac{\pi^2}{9} \exp\left(-\frac{4m_\chi}{m_\phi} \log\left(\frac{16}{9} \frac{m_\chi^2}{H_{\text{end}}^2}\right)\right). \quad (3.23)$$

This simple and instructive result shows that the gravitational production of the supermassive field χ grows with the mass of the inflaton field. However, it is essential to note that this approach breaks down when $m_\phi \gg m_\chi$. In that case, as shown in Fig. 2, the saddle points approach each other closely, making the approximation of a single saddle point in Eq. (3.23) invalid. The scenario of gravitational production for $m_\phi \gg m_\chi$ is discussed in [51, 76].

Numerical results

Depending on the inflaton mass m_ϕ , gravitational production of a heavy particle after inflation (when the inflaton oscillates around its minimum) can overcome the inflationary production. When $m_\phi \lesssim H_I$ ($\alpha \gtrsim 1$), the later contribution after inflation does not overshoot the inflationary production at Hubble crossing for IR modes $k < k_{\text{end}}$, and their final occupation number can be estimated as $n_k \sim \exp(-2\pi\nu(t_k))$. Conversely, if the inflaton mass is heavier than the Hubble scale ($\alpha \lesssim 1$), the oscillation of the inflaton at the end of inflation can lead to the production of heavy particles through gravitational preheating. In this scenario, the occupation number is approximately $n_k \sim \exp(-\mathcal{O}(1)m_\chi/m_\phi)$ as in Eq. (3.23). Note that the steepest descent method, used to evaluate the gravitational particle production during reheating period, $n_k \sim \exp(-\mathcal{O}(1)m_\chi/m_\phi)$, is not applicable when $m_\phi \gg m_\chi$, as previously explained. Given these distinct production mechanisms, we explore both regimes by presenting analytic and numerical results for each of them.

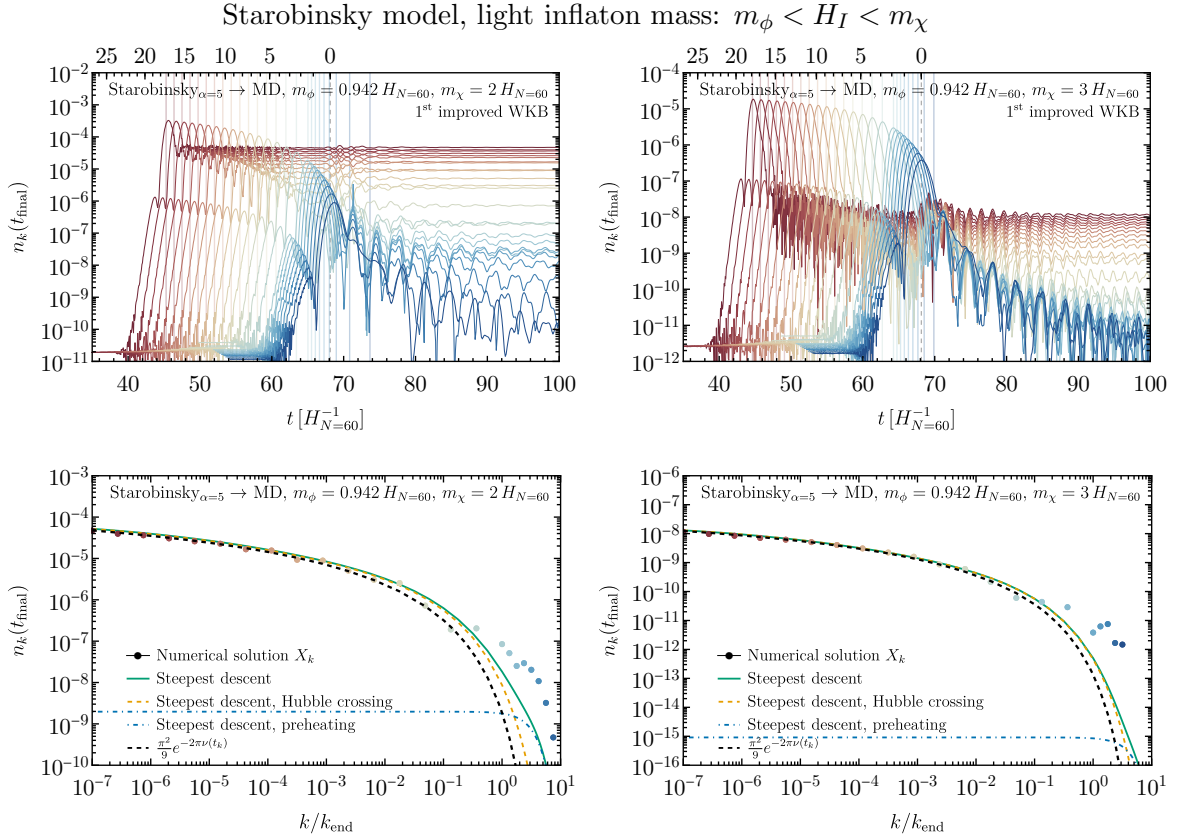


Figure 6. Same as Fig. 4, for the Starobinsky inflationary model with $\alpha = 5$. Here, we define $H_I \equiv H_{N=60}$ at 60 e -folds before the end of inflation. In the bottom panels, we show separately the production during inflation (‘Hubble crossing’, dashed yellow) and right after the end of inflation (‘preheating’, dot-dashed blue), along with their sum (solid green), estimated with the steepest descent approximation.

Light inflaton mass ($m_\phi \lesssim H_I$ or $\alpha \gtrsim 1$) We consider a light inflaton with $m_\phi \lesssim H_I < m_\chi$, resulting in suppressed particle production post-inflation. Here, the Hubble scale is defined at 60 e -folding before the end of inflation, $H_I = H_{N=60}$. In accordance to Eq. (3.19), a lighter inflaton mass corresponds to a larger value of α . As a benchmark model, we select $\alpha = 5$, which yields an inflaton mass m_ϕ (in its minimum at the end of inflation) smaller than the inflationary Hubble, $m_\phi = 0.94H_I$. We choose this value where the post-inflationary gravitational production has a very moderate impact on the spectrum of χ , in order to highlight the difference between the two regimes. We compare the numerical evaluation of the mode function X_k , with the analytic formula for particle production during inflation with a time-varying Hubble rate, expressed in Eq. (3.16), as well as with the numerical evaluation of the steepest descent method.

In the first numerical approach, we solve the evolution of the modes X_k within the Starobinsky background, and evaluate the occupation number using the 1st order improved WKB approximation. The results are presented in Fig. 6 with colored lines for each mode k for two scalar masses $m_\chi = 2, 3H_I$. The upper plots show n_k as a function of cosmic

time t for each mode, and the bottom plots show the corresponding value of n_k (with the same color code) at a late time $t = 200 H_I$ (with a time average over the small decreasing oscillations).

In the lower plots, the spectrum of the IR modes ($k \lesssim 0.1 k_{\text{end}}$, in red-orange) align very well with the analytical estimate of inflationary particle production with the steepest descent method, $n_k \simeq \frac{\pi^2}{9} \exp(-2\pi\nu(t_k))$ (black dashed line), as discussed in Section 3.2. We also estimate n_k by numerically finding the dominant poles during inflation and shortly after t_{end} , and performing the integral of Eq. (2.30). In order to do so, it is necessary to analytically extend $\omega_k(t)$. For the pole around Hubble crossing (see Fig. 2), one can easily fit the (slowly varying) Hubble rate with a polynomial in t , and compute the scale factor $a(t) \sim \exp(\int H(t))$. The analytical extension of $\omega_k(t)$ around the inflaton oscillations (blue band in 1) is more delicate: we perform a fit of $\phi(t) \sim \frac{1}{t-t_0} \cos(\omega_\phi t)$ around a few inflaton oscillations to take care of the term $\frac{9}{4}wH^2$ in $\omega_k(t)$, and fit $a \sim t^{2/3}$ for the gradient term $k^2/a^2(t)$. This numerical method yields consistent results in both the IR and UV region. The sum of the contributions from the two poles, as in Eq. (2.30), is depicted as a solid green line in the lower plots. For UV modes ($k > k_{\text{end}}$, marked as blue dots), particle production during inflation is exponentially suppressed in k , so that post-inflationary production becomes the dominant contribution. Finally, we notice that the occupation number derived through the steepest descent method underestimates the one obtained through the numerical solution of X_k . This may be due to the inaccuracy of the analytical extension of $\omega_k(t)$ in the complex t plane, which can hardly be fitted over a large enough time range on the real axis.

Heavy inflaton mass ($m_\phi \gtrsim H_I$ or $\alpha \lesssim 1$) We focus now the case where the inflaton mass in its minimum is large ($m_\phi \gtrsim H_I$), but m_ϕ is not significantly larger than the spectator field mass m_χ . Under these conditions, particle production primarily occurs *after* inflation for both UV and IR modes. We adopt $\alpha = 1$ as our benchmark model, which corresponds to an inflaton mass $m_\phi = 2.03H_I$. The numerical solutions, along with the results obtained with the steepest descent method, are summarized in Fig. 7. We show the results for two scalar masses: $m_\chi = 2H_I$ (left column) and $m_\chi = 3H_I$ (right column). The upper panels of the figure depict the rise in n_k immediately after the end of inflation ($t_{\text{end}} \approx 59 H_I$, corresponding to 0 e -folds until the end of inflation on the upper axis), indicating that the predominant particle production occurs after inflation, during the preheating phase. This observation is corroborated in the lower panel by comparing the numerical solution (red/blue colored points) with the lines obtained from the steepest descent method. The dotted black line (given by $n_k \simeq \frac{\pi^2}{9} \exp(-2\pi\nu(t_k))$) is consistent with the numerical evaluation of the saddle point approximation using only the saddle during inflation (dashed yellow line). The two lines are in agreement in the IR spectrum, while they show some deviation in the UV spectrum. Moreover, post-inflation particle production, as determined by the steepest descent method, is several orders of magnitude greater than inflation production. For $m_\chi = 2H_I$, numerical solutions for X_k (red-blue points) agree with the steepest descent method (green line), whereas for $m_\chi = 3H_I$, the prediction from the steepest descent method is slightly smaller. This discrepancy for large

Starobinsky model, heavy inflaton mass: $H_I < m_\phi < m_\chi$

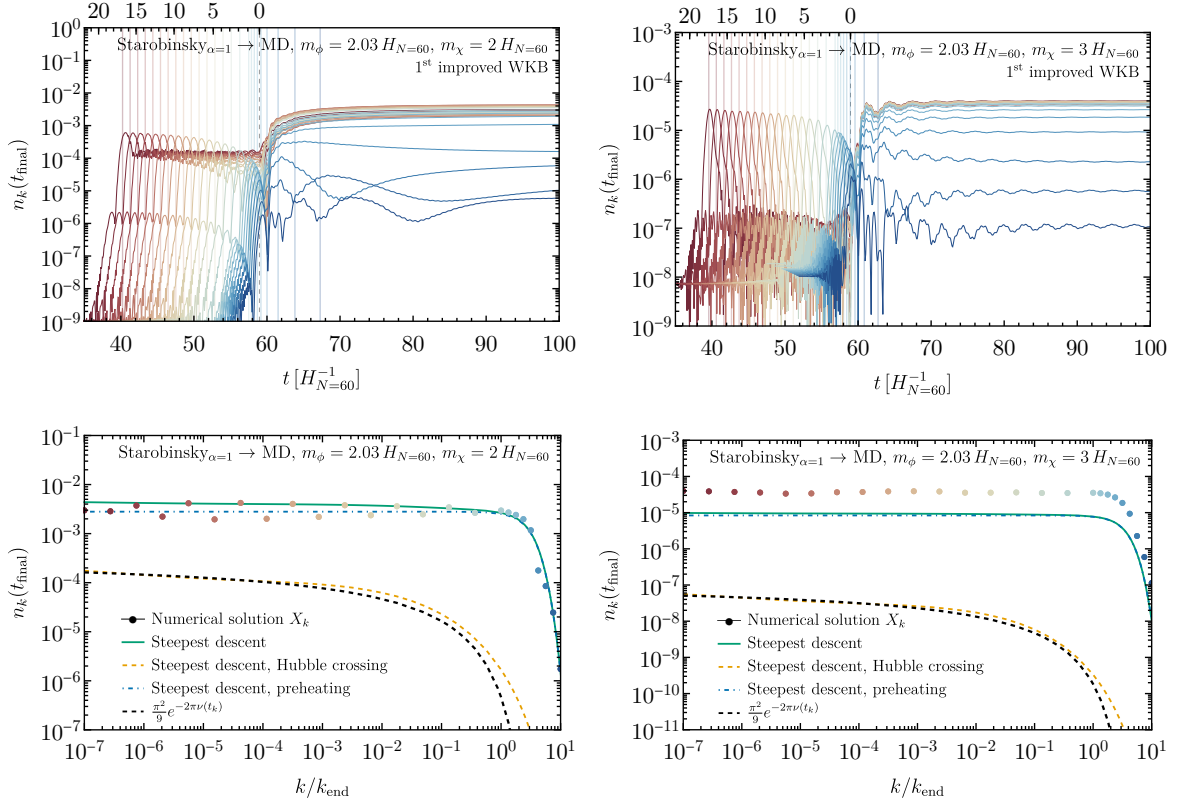


Figure 7. Same as in Fig. 6, for the case of heavier inflaton $m_\phi = 2.03H_I$ ($\alpha = 1$) in the Starobinsky model. When the inflaton mass m_ϕ in its minimum is larger than the inflationary Hubble rate (but smaller than m_χ , post-inflationary gravitational production can overcome the inflationary production, with an occupation number in the IR mode (red-orange lines and dots) $n_k \sim \exp(-\mathcal{O}(1)m_\phi/m_\chi)$. The dot-dashed blue lines in the bottom plots highlight the impact of post-inflationary gravitational production with respect to the inflationary one (dashed yellow line).

m_χ is expected, because it implies a wider extrapolation from the value $\omega_k \sim m_\chi$ on the real t axis (see Fig. 1) to $\omega_k(t_n) = 0$ in the complex plane (see Fig. 2). This results in an amplification of the error of the analytic continuation of $\omega_k(t)$.

Finally, to illustrate the influence of inflaton mass, and thus the model dependence, on the post-inflationary gravitational production, we plot the occupation number n_k against momentum k for four different values of m_ϕ/H_I in Fig. 8 (with the same spectator mass $m_\chi = 2H_I$). The inflaton mass dependence is represented by various values of α (1, 3, 4, and 5) in the four panels. The dashed blue lines show the increase with m_ϕ (or decrease with α) of the post-inflationary particle production.

4 Reheating and Dark Matter Abundance

The goal of this section is to compute the present abundance of the gravitationally produced χ , in order to assess the parameter space where it can form the totality of dark matter.

Occupation numbers of a superheavy χ in the Starobinsky model for decreasing m_ϕ/H_I

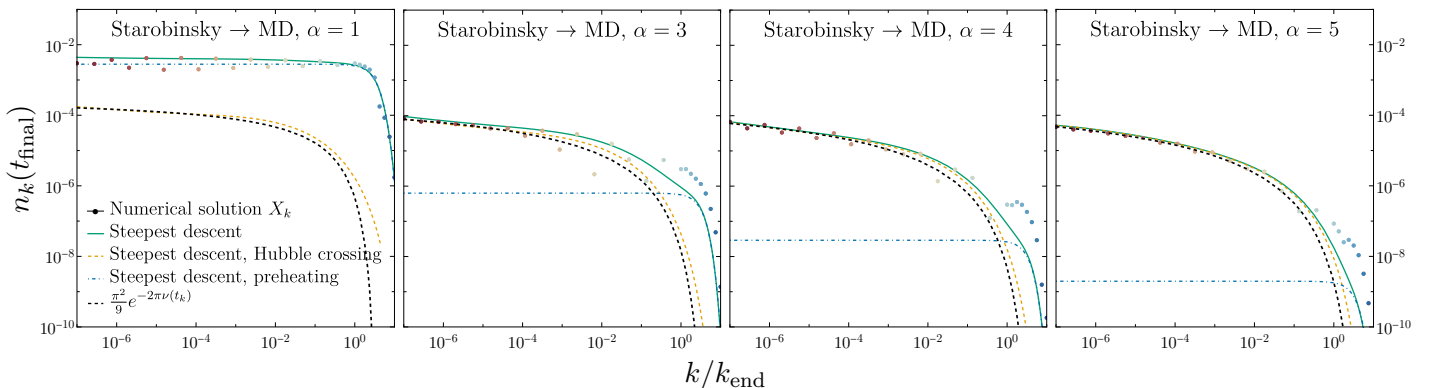


Figure 8. Comparison of the particle production for decreasing values of the inflaton mass in units of H_I (respectively $m_\phi = 2.0, 1.2, 1.0, 0.9 H_I$, corresponding to increasing $\alpha = 1, 3, 4, 5$ in the Starobinsky model), with the same color code as the bottom panels of Fig. 6 and 7. For all plots, the spectator field mass is $m_\chi = 2H_{N=60}$. The inflationary production (dashed yellow and black lines) stays the same in the four cases, while the post-inflationary production decreases, as shown by the red-blue points (numerical solution of the modes X_k) and the solid green line (steepest descent approximation).

We first discuss the reheating epoch that occurs immediately after the end of inflation in a matter-dominated universe. After t_{end} , as the inflaton decays, the thermal plasma dilutes until it reaches a maximum temperature T_{max} [94]. Subsequently, the temperature decreases until reheating, which occurs when the energy density of the inflaton becomes equal to the energy density of radiation, $\rho_\phi(a_{\text{RH}}) = \rho_R(a_{\text{RH}})$. The reheating temperature can be expressed as a function of the inflaton decay rate Γ_ϕ as [95, 96]

$$\frac{\pi^2 g_{*,\text{RH}} T_{\text{RH}}^4}{30} \simeq 3 \left(\frac{2}{5} \Gamma_\phi M_{\text{P}} \right)^2 \Rightarrow T_{\text{RH}} \simeq 1.7 \times 10^{15} \text{ GeV} \cdot g_{*,\text{RH}}^{-1/4} \cdot \left(\frac{\Gamma_\phi}{10^{12} \text{ GeV}} \right)^{1/2}, \quad (4.1)$$

where $g_{*,\text{RH}}$ is the total number of relativistic degrees of freedom of the thermal bath at T_{RH} .

For the case of superheavy dark matter that we consider in this paper, the number-density $\frac{1}{2\pi^2} k^3 n_k$ is blue-tilted, and the abundance is dominated by the modes around the Hubble radius towards the end of inflation, with $k/k_{\text{end}} \sim \mathcal{O}(1 - 10)$. The shorter-wavelength UV tail, with $k/k_{\text{end}} > 10$, is exponentially suppressed, as shown by Eq. (3.8). We can evaluate the particle occupation number $n_k = |\beta_k|^2$ at some time after the end of inflation, when the comoving number density $n_{\chi,\text{co}}$ is constant:

$$n_\chi(t) a(t)^3 = \frac{1}{2\pi^2} \int_0^\infty dk k^2 |\beta_k|^2 \equiv n_{\chi,\text{co}} = \text{const.}, \quad (4.2)$$

where $n_\chi(t)$ is the physical number density and $a(t)$ is the scale factor at a time $t > t_{\text{end}}$ when the particle number density remains constant. We evaluate the comoving particle number density numerically to compute the present-day dark matter abundance.

The reheating phase is complete when the energy density of the inflaton ρ_ϕ becomes equal to the energy density of radiation ρ_R :

$$\rho_R(a_{\text{RH}}) = \rho_\phi(a_{\text{RH}}) = \rho_\phi(a_{\text{end}}) \left(\frac{a_{\text{end}}}{a_{\text{RH}}} \right)^3 = 3M_{\text{P}}^2 H_{\text{end}}^2 \left(\frac{a_{\text{end}}}{a_{\text{RH}}} \right)^3. \quad (4.3)$$

After a_{RH} , the universe becomes radiation-dominated and the dark matter yield remains constant:

$$Y_\chi(a_{\text{RH}}) \equiv \frac{n_\chi(a_{\text{RH}})}{s(a_{\text{RH}})} = \frac{n_{\chi,\text{co}} a_{\text{end}}^{-3} T_{\text{RH}}}{4M_{\text{P}}^2 H_{\text{end}}^2}, \quad (4.4)$$

where we introduced the entropy density $s(T) = \frac{2\pi^2}{45} g_* T^3$ and we used Eq. (4.2) and Eq. (4.3). The present relic abundance of dark matter is given by

$$\Omega_\chi h^2 = \frac{\rho_\chi(a_0)}{\rho_{\text{cr}}} = \frac{m_\chi n_\chi(a_0)}{\rho_{\text{cr}}} h^2 = \frac{m_\chi Y_\chi(a_{\text{RH}}) s_0}{\rho_{\text{cr}}} h^2, \quad (4.5)$$

where a_0 is the scale factor today, $\rho_{\text{cr}} = 1.054 \times 10^{-5} h^2 \text{ GeV cm}^{-3}$ is the critical density today, $h = H_0/(100\text{km/s/Mpc})$ and $s_0 = 2891.2 \text{ cm}^{-3}$ is the present entropy density. Using Eq. (4.1), we finally obtain

$$\begin{aligned} \Omega_\chi h^2 &= 6.9 \cdot 10^7 \left(\frac{m_\chi}{\text{GeV}} \right) \left(\frac{n_{\chi,\text{co}} a_{\text{end}}^{-3} T_{\text{RH}}}{M_{\text{P}}^2 H_{\text{end}}^2} \right) = \\ &= 0.12 \left(\frac{g_{*,\text{RH}}}{106.75} \right)^{-1/4} \frac{n_{\chi,\text{co}}}{6 \cdot 10^{-10} k_{\text{end}}^3} \frac{m_\chi}{H_{\text{end}}} \left(\frac{\Gamma_\phi}{10^{-3} H_{\text{end}}} \right)^{1/2} \left(\frac{H_{\text{end}}}{10^{12} \text{ GeV}} \right)^{5/2}. \end{aligned} \quad (4.6)$$

We are now able to compute the present abundance for the gravitationally produced dark matter in two of the models considered in this paper. We illustrate the integrand of the number density in Eq. (4.2) in Fig. 9 for the inflationary models of de Sitter (Section 3.1) and Starobinsky (Section 3.3). In the top panels, we show (for two dark matter masses $m_\chi = 2H_I$ and $3H_I$) the numerical solution (red/blue dots) of the model $\text{dS} \rightarrow \text{Minkowski}$, together with the steepest descent approximation (green line). The two methods are in excellent agreement. The slope of the integrand scales as $(k/k_{\text{end}})^2 \cdot n_k(t_{\text{final}}) \propto k^2$ for the IR modes $k \ll k_{\text{end}}$, while the UV tail $k \gg k_{\text{end}}$ is exponentially suppressed. The bottom panels show the same results for the model of Starobinsky inflation with $\alpha = 1$ (case of heavy inflaton mass, with significant post-inflationary production). As discussed at the end of Section 3.3, the green line for the steepest descent method offers a worse approximation of the result at larger m_χ , because of the bigger extrapolation that is implied in the analytical extension of $\omega_k(t)$.

The total comoving number density of dark matter particles in the de Sitter model can be fitted by

$$n_{\chi,\text{co}} \simeq \frac{1.3}{6\pi^2} k_{\text{end}}^3 e^{-2\pi\nu} \quad (\text{de Sitter inflation}), \quad (4.7)$$

as shown in Fig. 10 together with the points computed with the saddle point approximation. The corresponding dark matter abundance from Eq. (4.6) is

$$\Omega_\chi h^2 \simeq 1.5 \times 10^6 e^{-2\pi\nu} \left(\frac{m_\chi}{\text{GeV}} \right) \left(\frac{H_{\text{end}} T_{\text{RH}}}{M_{\text{P}}^2} \right) \quad (\text{de Sitter inflation}). \quad (4.8)$$

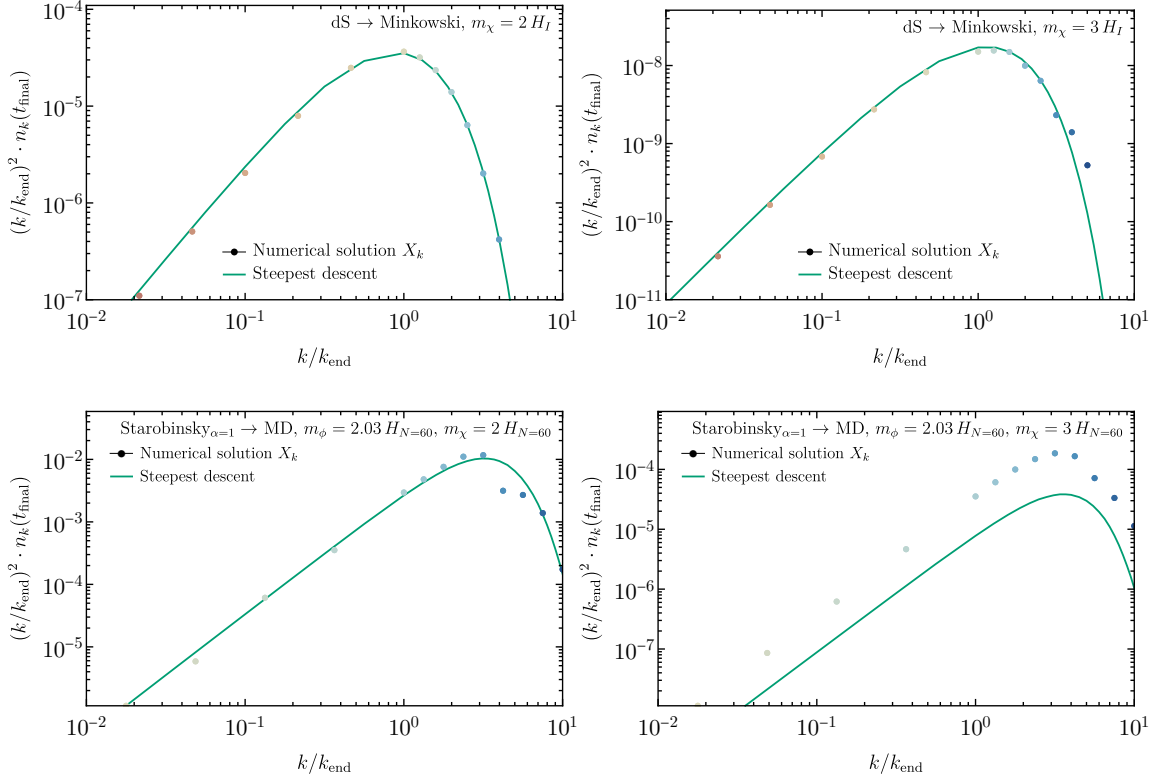


Figure 9. The phase space distribution $(k/k_{\text{end}})^2 \cdot n_k(t_{\text{final}})$ of the integral (4.2) as a function of k/k_{end} for the pure de Sitter model (top panels) and the Starobinsky model with post-inflationary production (bottom panels). The solid green line shows the steepest descent approximation.

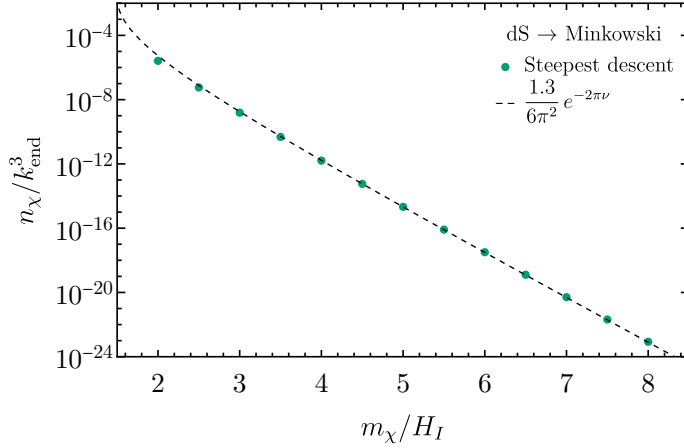


Figure 10. Total comoving number density $n_{\chi, \text{co}}$ of superheavy particles in the de Sitter inflationary model, and fit with the formula in Eq. (4.7).

Imposing the observed dark matter constraint $\Omega_{\chi} h^2 \simeq 0.12$, we obtain the relation between

$H_{\text{end}}, T_{\text{RH}}, m_\chi$ that gives the correct dark matter abundance:

$$T_{\text{RH}} \simeq 4.7 \cdot 10^{14} \text{ GeV} \cdot \frac{10^{-9}}{e^{-2\pi\nu}} \cdot \frac{(10^{12} \text{ GeV})^2}{m_\chi H_{\text{end}}} \quad (\text{de Sitter inflation}). \quad (4.9)$$

The reheating temperature T_{RH} can be traded for the inflaton decay rate Γ_ϕ through Eq. (4.1). We can further relate Γ_ϕ to the Hubble rate H_{end} , because $m_\phi \sim H_{\text{end}}$, and the decay rate Γ_ϕ can be related via dimensional arguments to $m_\phi \sim H_{\text{end}}$. We can then introduce the ratio $\Gamma_\phi/H_{\text{end}}$, which quantifies the strength of preheating and the size of the inflaton couplings (for a perturbative decay rate controlled by a coupling y , and taking $m_\phi \sim H_{\text{end}}$, we would have $\Gamma_\phi/H_{\text{end}} \sim y^2/(8\pi)$). This leaves us with two free parameters: m_χ , and T_{RH} or H_{end} . We show in Fig. 11 the dark matter abundance for the de Sitter

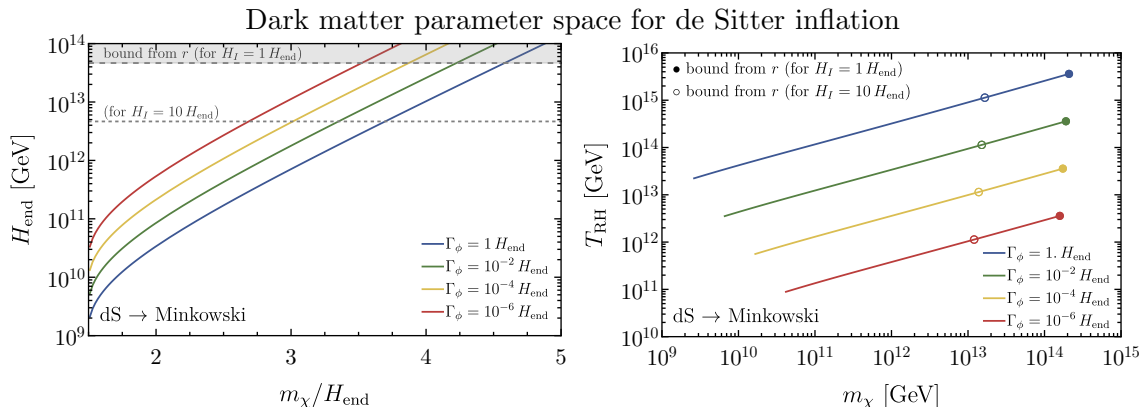


Figure 11. Parameter space for gravitationally produced superheavy dark matter in the de Sitter inflationary model. The observed relic abundance is achieved when Eq. (4.9) is satisfied, and the parameters T_{RH} and H_{end} can be related through the inflaton decay rate Γ_ϕ . We trade one of the two parameters (T_{RH} on the *left* plot, H_{end} on the *right*) for different assumptions on the strength of reheating $\Gamma_\phi/H_{\text{end}}$. We also show with dashed horizontal lines (*left*) and dots (*right*) the upper limits on the inflationary H_I , and on T_{RH} on the right plot, from Planck/BICEP, assuming $H_I = 1, 10 H_{\text{end}}$. In both plots, the end-points of the colored curves at low m_χ mark the regime of massive $m_\chi > \frac{3}{2} H_I$ that we assume in our analysis.

inflationary model for these two choices. The left panel refers to the inflationary quantities m_χ/H_{end} and H_{end} , and shows the dark matter abundance for different choices of $\Gamma_\phi/H_{\text{end}}$ and two values of H_I/H_{end} . The corresponding upper limit on H_I of Planck and BICEP from the non-detection of primordial B-modes in the CMB polarisation ($r < 0.036$ at 95% CL [97]) is shown with horizontal dashed lines. The right panel shows the same curves in the parameter space (m_χ, T_{RH}) , with the dots marking the upper limits on H_I . In both plots, the limiting points on the left correspond to $m_\chi = 3H_I/2$, below which our analysis for superheavy spectator fields does not apply.

For the Starobinsky model of inflation discussed in Section 3.3, we compute the total number density from the numerical results obtained by evolving the mode equations for X_k (shown in Figs. 7 and 9). The results is shown in Fig. 12, and the case $\alpha = 1$ is well fitted by

$$n_{\chi, \text{co}} \simeq \frac{76}{6\pi^2} k_{\text{end}}^3 e^{-0.55\pi\nu} \quad (\text{Starobinsky inflation, } \alpha = 1). \quad (4.10)$$

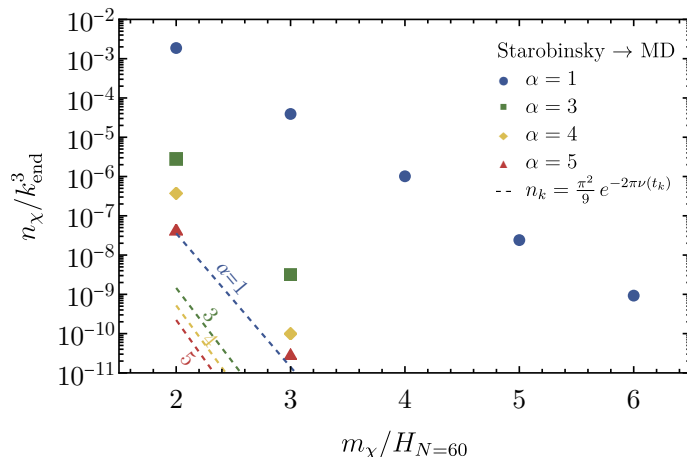


Figure 12. Total comoving number density $n_{\chi, \text{co}}$ of superheavy particles in the Starobinsky inflationary mode, computed with the numerical results of the evolution of the mode functions X_k . Decreasing values of α (marked with different colors and point markers) correspond to increasing the inflaton mass in its minimum in Hubble units, and thus enhancing the post-inflationary production. The dashed lines show for each α (with the same color code) the predicted abundance if the post-inflationary production is neglected. The dots for $\alpha = 1$ are well fitted by Eq. (4.10).

The exponential suppression featured in realistic inflationary models is milder than the standard $\exp(-2\pi\nu)$ for inflationary production at Hubble crossing, as a result of the enhanced production after the end of inflation (especially for larger inflaton masses). The UV tail $k \gtrsim k_{\text{end}}$ dominates this result, as visible in Fig. 9, and increases by a factor $\sim \mathcal{O}(1)$ the predicted mass for dark matter. The relic abundance obtained from Eq. (4.6) is

$$\Omega_\chi h^2 \simeq 8.9 \times 10^7 e^{-0.55\pi\nu} \left(\frac{m_\chi}{\text{GeV}} \right) \left(\frac{H_{\text{end}} T_{\text{RH}}}{M_{\text{p}}^2} \right) \quad (\text{Starobinsky inflation, } \alpha = 1), \quad (4.11)$$

which can be re-expressed in terms of the reheating temperature T_{RH} as

$$T_{\text{RH}} \simeq 8.0 \cdot 10^{12} \text{ GeV} \cdot \frac{10^{-9}}{e^{-0.55\pi\nu}} \cdot \frac{(10^{12} \text{ GeV})^2}{m_\chi H_{\text{end}}} \quad (\text{Starobinsky inflation, } \alpha = 1). \quad (4.12)$$

In conclusion, in a realistic inflationary model where post-inflationary production of a heavy spectator field could be larger than the inflationary production at Hubble crossing, the right mass range for DM increases from $\sim 1-4 H_{\text{end}}$ (Fig. 11) to $\sim 2-14 H_{\text{end}}$ (Fig. 13).

5 Discussion and Conclusions

We have investigated the gravitational production of superheavy scalar fields with mass $m_\chi \gtrsim H_I$ during and after inflation. This phenomenon arises inevitably due to gravitational interactions, and provides a minimal setup for dark matter production.

We focus on an analytical approach to the calculation of the produced particle abundance, by means of the steepest-descent approximation. Besides the computational advantage in performing this calculation with respect to the numerical time evolution of the

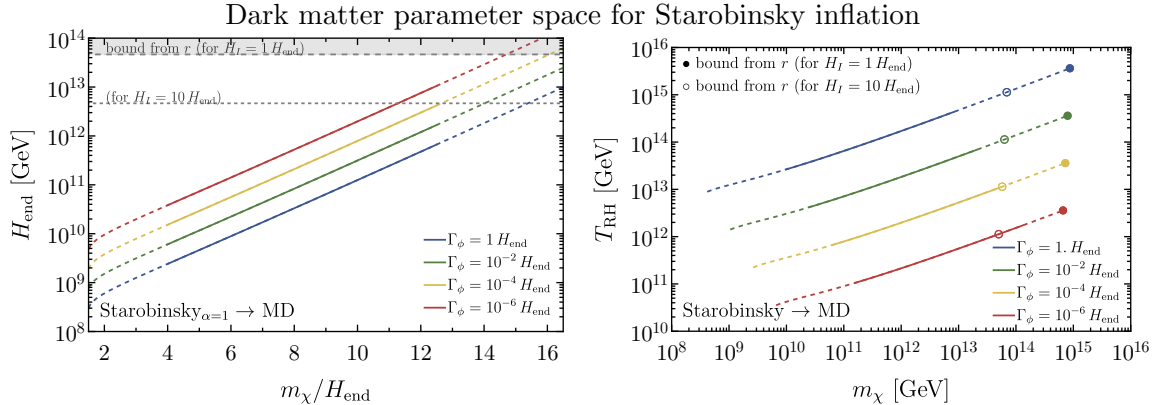


Figure 13. Same as Fig. 11, for the model of Starobinsky inflation with $\alpha = 1$, corresponding to heavy inflaton mass and predominant post-inflationary production. The lines for the correct relic abundance of dark matter are shown with a solid line when they fall within the range of the points that we computed explicitly (shown in Fig. 12), and with a dashed line when they rely on the extrapolation of Eq. (4.10).

mode functions, we have highlighted the conceptual clarifications that emerge in this picture. As a first step, the epochs of gravitational production can be easily identified by solving for $\omega_k(t) = 0$ with complex t (see Fig. 1), pointing to the times around Hubble exit and at the end of inflation, when the inflaton oscillates in this minimum. In this approach, these different production phases emerge from a simple and coherent picture. Second, the exponent in the suppressed particle abundance can be estimated directly from the expression of $\omega_k(t)$ (see Fig. 2). This allows to derive in a few lines known results for the particle occupation number ($e^{-2\pi\nu}$ for de Sitter, with $\nu = \sqrt{m_\chi^2/H^2 - 9/4}$), and to derive novel results as Eqs. (3.8), (3.16) and (3.23) in a simple fashion. We find that the production during inflation (with a slowly-evolving H) leads to $e^{-2\pi\nu(t_k)}$ with $\nu(t_k)$ evaluated when the physical mode is still inside the Hubble radius (Eq. (3.16)), and that post-inflationary production can be captured by $e^{-\mathcal{O}(1)m_\chi/m_\phi}$ (Eq. (3.8)). As the inflaton mass m_ϕ increases, production after inflation becomes the dominant contribution.

We explored three inflationary scenarios: de Sitter transitioning to Minkowski, power-law inflation, and the Starobinsky model of inflation. The agreement between our analytical and numerical results validates this method and extends the applicability of our analytical techniques for various models of inflation. We notice that our results can be applied to the gravitational production of superheavy fermions and vectors, which obey a similar dispersion relation as scalars, leading to an exponentially-suppressed particle number density for inflationary production.

We also explored scenarios in which gravitationally produced heavy scalars are a viable dark matter candidate, assuming their stability over cosmological timescales. For superheavy scalar production with $m_\chi \gtrsim H_I$, the gravitational particle production is sensitive to the transition from the inflationary phase to the matter-dominated phase. We modeled the dynamics using the Starobinsky model of inflation, characterized by a variable parameter α , that governs the steepness of this transition. For large-scale inflation ($H_I \gtrsim 10^9$ GeV)

and relatively high reheating temperature, heavy spectators fields ($m_\chi \sim \mathcal{O}(1 - 10)H_{\text{end}}$) can naturally account for the observed dark matter. Such a candidate is particularly compelling from a phenomenological perspective as they avoid isocurvature constraints, with $m_\chi \gtrsim 0.5H_I$, and may lead to cosmological collider signatures or primordial gravitational waves (tensor modes), a prospect that future experiments will be able to explore. Although the prospects for terrestrial detection of such a dark matter candidate are weaker, there are ideas in this direction as well. The Windchime Project [98, 99] proposes to employ an array of mechanical sensors configured to function as a single detector. This setup is designed to detect subtle disturbances caused by superheavy dark matter as it interacts with these sensors. This experiment is most sensitive to masses approaching or exceeding the Planck scale, but it may be improved in the future to detect lower mass, possibly related to inflationary particle production. Looking ahead, we eagerly anticipate developments in our theoretical understanding of inflationary physics and upcoming CMB and large-scale structure surveys, which can advance our understanding of the early universe, and provide us with new insights about the nature of dark matter.

Acknowledgments

We thank Valerie Domcke, Marcos A. G. García, Yohei Ema, Rocky Kolb, Marco Peloso, Riccardo Penco, Mathias Pierre, Michele Redi, Antonio Riotto, Leonardo Senatore and Richard Woodard for useful discussions and comments. D.R. is supported in part by NSF Grant PHY-2014215, DOE HEP QuantISED award #100495, and the Gordon and Betty Moore Foundation Grant GBMF7946. D.R. acknowledges hospitality from the Perimeter Institute for Theoretical Physics during the preparation of this paper. Research at Perimeter Institute is supported in part by the Government of Canada through the Department of Innovation, Science and Economic Development Canada and by the Province of Ontario through the Ministry of Colleges and Universities. S.V. and W.X. are supported in part by the U.S. Department of Energy under grant DE-SC0022148 at the University of Florida.

A WKB Approximation

In this appendix, we briefly discuss the higher-order WKB approximation. To ensure numerical precision in our particle abundance spectra, we primarily utilize the first improved WKB order in most of our plots and analyses. For a detailed discussion on generating higher-order terms in the adiabatic expansion, see Ref. [87].

One can demonstrate that for an adiabatic expansion of the form

$$\chi_k(t) = \frac{1}{\sqrt{W_k(t)}} e^{-i \int^t W_k}, \quad (\text{A.1})$$

to satisfy the equation of motion (2.9), it is necessary for $W_k(t)$ to satisfy the following constraint

$$W_k^2(t) = \omega_k^2(t) + \sqrt{W_k(t)} \frac{d^2}{dt^2} \left(\frac{1}{\sqrt{W_k(t)}} \right). \quad (\text{A.2})$$

Therefore, we can iteratively solve this expression to determine the j -th order of the adiabatic expansion. Up to the second improved order, we obtain

$$\omega_k^{(0)}(t) = \omega_k(t), \quad (\text{A.3})$$

$$\omega_k^{(1)}(t) = \omega_k(t) - \frac{1}{4} \left(\frac{\ddot{\omega}_k}{\omega_k^2} - \frac{3 \dot{\omega}_k^2}{2 \omega_k^3} \right), \quad (\text{A.4})$$

$$\omega_k^{(2)}(t) = \omega_k(t) - \frac{1}{4} \left(\frac{\ddot{\omega}_k}{\omega_k^2} - \frac{3 \dot{\omega}_k^2}{2 \omega_k^3} \right) - \frac{1}{8} \left(\frac{13 \ddot{\omega}_k^2}{4 \omega_k^5} - \frac{99 \dot{\omega}_k^2 \ddot{\omega}_k}{4 \omega_k^6} + 5 \frac{\dot{\omega}_k \ddot{\omega}_k}{\omega_k^5} + \frac{1}{2} \frac{\ddot{\omega}_k}{\omega_k} - \frac{297 \dot{\omega}_k^4}{16 \omega_k^7} \right). \quad (\text{A.5})$$

At the $(j+1)$ -th order of expansion, we find

$$\omega_k^{(j+1)} = \sqrt{\omega_k^2 - \left[\frac{\ddot{\omega}_k^{(j)}}{2\omega_k^{(j)}} - \frac{3}{4} \left(\frac{\dot{\omega}_k^{(j)}}{\omega_k^{(j)}} \right)^2 \right]}, \quad (\text{A.6})$$

truncated at the order of at most $2j$ derivatives with respect to time. Importantly, the final results evaluated at asymptotic time limit $t_f \rightarrow \infty$ are independent of the order of the WKB approximation, as the basis-dependent terms vanish in this limit.

B Stokes Line Approach

In this appendix, we compare method of steepest descent approximation with the Stokes line approach. The latter was considered in the context of the Schwinger effect [87, 88], and has been applied in the context of gravitational particle production [74, 75, 80]. We note that when $m_\chi \gtrsim H_I$, from Eq. (2.10) we see that $\nu^2 \gg 0$ and $\omega_k^2 \gtrsim 0$ is always positive. This allows us to approximate the location of the saddle points as

$$a(t_0) \simeq \pm \frac{ik}{m_\chi}. \quad (\text{B.1})$$

In this work, we explored the WKB approximation for estimating the Bogoliubov coefficients and particle abundance [51, 69, 77, 86, 100] and focused on the steepest descent approximation. However, as argued in [101], the mode functions evolve substantially during the expansion of the universe and this necessitates to identify the dominant and subdominant contributions of the WKB approximation linked to particle production. As discussed in [87], to fully account for the contribution arising from the negative frequency subdominant component, one needs to consider Stokes phenomenon.

Recently, these concerns were studied in detail in Ref. [75]. The discrepancy between the WKB approximation and the Stokes phenomenon arises because the WKB adiabatic expansion can only be defined locally. This implies that mode functions at some initial time t_i cannot be analytically extended across the entire complex plane, and the WKB approximation breaks down close to the poles (saddle points), where the adiabaticity conditions become violated. Thus, as the contour passes through a Stokes line, which characterizes the region where the local approximation is valid, the negative frequency contribution must be incorporated into the WKB solution.

The Stokes lines are determined by the condition

$$F_k(t) \equiv -2i \int_{t_n}^t \omega_k(t') dt' = \text{purely real}, \quad (\text{B.2})$$

where t_n denotes the location of the saddle point $\omega(t_n) = 0$ lying in the lower half-plane. One can show that the Bogoliubov coefficient can be approximated as [87, 102, 103]

$$\beta_k(t) \simeq -i S_k(t) e^{i \int_{t_n}^{t_n^*} \omega_k(t') dt'}, \quad (\text{B.3})$$

with the Stokes multiplier defined as

$$S_k(t) \equiv \frac{1}{2} \left[1 + \operatorname{erf} \left(-\frac{\operatorname{Im} F_k(t)}{\sqrt{2} |\operatorname{Re} F_k(t)|} \right) \right]. \quad (\text{B.4})$$

Given that the error function varies between -1 and 1 , we observe that $\beta_k(t)$ transitions from 0 to $i e^{i \int_{t_n}^{t_n^*} \omega_k(t') dt'}$. We now compare it with the steepest descent approximation. From Eq. (B.1), we observe that for superheavy dark matter, the saddle points lie in the complex plane. Consequently, the exponential term can be estimated as $e^{i \int_{t_n}^{t_n^*} \omega_k(t') dt'} = e^{-2i \int_{\operatorname{Re} t_n}^{t_n} \omega_k(t') dt'}$. The integral in the exponential term coincides with Eq. (2.31) employed in the steepest descent method. The primary difference between these methods lies in the prefactor. However, as the steepest descent approximation yields a prefactor of $\pi^2/9 \simeq 1$ for the coefficient $|\beta_k|^2$, it nearly matches the peak value of the Stokes multiplier $S_k(t) \simeq 1$, and the two approaches lead to nearly identical results. Consequently, in our analysis, we favor the simpler steepest descent approximation over evaluating the Stokes multiplier. For a comparison of the steepest descent method with the Stokes phenomenon, see Ref. [79], and for a detailed exploration of superheavy scalar field production using the Stokes phenomenon, see Ref. [74].

References

- [1] D. H. Lyth and A. Riotto, *Particle physics models of inflation and the cosmological density perturbation*, *Phys. Rept.* **314** (1999) 1 [[hep-ph/9807278](#)].
- [2] L. Senatore, *Lectures on Inflation*, in *Theoretical Advanced Study Institute in Elementary Particle Physics: New Frontiers in Fields and Strings*, pp. 447–543, 2017, [1609.00716](#), DOI.
- [3] D. Baumann, *Primordial Cosmology*, *PoS TASI2017* (2018) 009 [[1807.03098](#)].
- [4] L. Parker, *Particle creation in expanding universes*, *Phys. Rev. Lett.* **21** (1968) 562.
- [5] L. Parker, *Quantized fields and particle creation in expanding universes. 1.*, *Phys. Rev.* **183** (1969) 1057.
- [6] L. Parker, *Quantized fields and particle creation in expanding universes. 2.*, *Phys. Rev. D* **3** (1971) 346.
- [7] L. H. Ford, *Cosmological particle production: a review*, *Rept. Prog. Phys.* **84** (2021) [[2112.02444](#)].

- [8] E. W. Kolb and A. J. Long, *Cosmological gravitational particle production and its implications for cosmological relics*, [2312.09042](#).
- [9] D. J. H. Chung, E. W. Kolb and A. Riotto, *Superheavy dark matter*, *Phys. Rev. D* **59** (1998) 023501 [[hep-ph/9802238](#)].
- [10] D. J. H. Chung, E. W. Kolb and A. Riotto, *Nonthermal supermassive dark matter*, *Phys. Rev. Lett.* **81** (1998) 4048 [[hep-ph/9805473](#)].
- [11] E. W. Kolb, D. J. H. Chung and A. Riotto, *WIMPzillas!*, *AIP Conf. Proc.* **484** (1999) 91 [[hep-ph/9810361](#)].
- [12] S. Ling and A. J. Long, *Superheavy scalar dark matter from gravitational particle production in α -attractor models of inflation*, *Phys. Rev. D* **103** (2021) 103532 [[2101.11621](#)].
- [13] M. A. G. Garcia, M. Pierre and S. Verner, *New window into gravitationally produced scalar dark matter*, *Phys. Rev. D* **108** (2023) 115024 [[2305.14446](#)].
- [14] D. H. Lyth and D. Roberts, *Cosmological consequences of particle creation during inflation*, *Phys. Rev. D* **57** (1998) 7120 [[hep-ph/9609441](#)].
- [15] V. Kuzmin and I. Tkachev, *Matter creation via vacuum fluctuations in the early universe and observed ultrahigh-energy cosmic ray events*, *Phys. Rev. D* **59** (1999) 123006 [[hep-ph/9809547](#)].
- [16] D. J. H. Chung, L. L. Everett, H. Yoo and P. Zhou, *Gravitational Fermion Production in Inflationary Cosmology*, *Phys. Lett. B* **712** (2012) 147 [[1109.2524](#)].
- [17] P. W. Graham, J. Mardon and S. Rajendran, *Vector Dark Matter from Inflationary Fluctuations*, *Phys. Rev. D* **93** (2016) 103520 [[1504.02102](#)].
- [18] A. Ahmed, B. Grzadkowski and A. Socha, *Gravitational production of vector dark matter*, *JHEP* **08** (2020) 059 [[2005.01766](#)].
- [19] E. W. Kolb and A. J. Long, *Completely dark photons from gravitational particle production during the inflationary era*, *JHEP* **03** (2021) 283 [[2009.03828](#)].
- [20] M. Gorghetto, E. Hardy, J. March-Russell, N. Song and S. M. West, *Dark photon stars: formation and role as dark matter substructure*, *JCAP* **08** (2022) 018 [[2203.10100](#)].
- [21] J. A. R. Cembranos, L. J. Garay, A. Parra-López and J. M. Sánchez Velázquez, *Vector dark matter production during inflation and reheating*, *JCAP* **02** (2024) 013 [[2310.07515](#)].
- [22] O. Özsoy and G. Tasinato, *Vector dark matter, inflation and non-minimal couplings with gravity*, [2310.03862](#).
- [23] F. Hasegawa, K. Mukaida, K. Nakayama, T. Terada and Y. Yamada, *Gravitino Problem in Minimal Supergravity Inflation*, *Phys. Lett. B* **767** (2017) 392 [[1701.03106](#)].
- [24] I. Antoniadis, K. Benakli and W. Ke, *Salvage of too slow gravitinos*, *JHEP* **11** (2021) 063 [[2105.03784](#)].
- [25] K. Kaneta, W. Ke, Y. Mambrini, K. A. Olive and S. Verner, *Gravitational production of spin-3/2 particles during reheating*, *Phys. Rev. D* **108** (2023) 115027 [[2309.15146](#)].
- [26] G. Casagrande, E. Dudas and M. Peloso, *On energy and particle production in cosmology: the particular case of the gravitino*, [2310.14964](#).
- [27] E. W. Kolb, S. Ling, A. J. Long and R. A. Rosen, *Cosmological gravitational particle production of massive spin-2 particles*, *JHEP* **05** (2023) 181 [[2302.04390](#)].

- [28] C. Gross, S. Karamitsos, G. Landini and A. Strumia, *Gravitational Vector Dark Matter*, *JHEP* **03** (2021) 174 [[2012.12087](#)].
- [29] M. Redi, A. Tesi and H. Tillim, *Gravitational Production of a Conformal Dark Sector*, *JHEP* **05** (2021) 010 [[2011.10565](#)].
- [30] G. Krnjaic, *Dark Radiation from Inflationary Fluctuations*, *Phys. Rev. D* **103** (2021) 123507 [[2006.13224](#)].
- [31] A. Arvanitaki, S. Dimopoulos, M. Galanis, D. Racco, O. Simon and J. O. Thompson, *Dark QED from inflation*, *JHEP* **11** (2021) 106 [[2108.04823](#)].
- [32] M. Redi and A. Tesi, *Dark photon Dark Matter without Stueckelberg mass*, *JHEP* **10** (2022) 167 [[2204.14274](#)].
- [33] M. Redi and A. Tesi, *Jump starting the dark sector with a phase transition*, *JHEP* **01** (2023) 085 [[2210.03108](#)].
- [34] W. E. East and J. Huang, *Dark photon vortex formation and dynamics*, *JHEP* **12** (2022) 089 [[2206.12432](#)].
- [35] M. Bastero-Gil, P. B. Ferraz, L. Ubalde and R. Vega-Morales, *Super heavy dark matter from inflationary Schwinger production*, [2311.09475](#).
- [36] M. Bastero-Gil, P. B. Ferraz, L. Ubalde and R. Vega-Morales, *Schwinger dark matter production*, [2312.15137](#).
- [37] D. J. H. Chung, E. W. Kolb, A. Riotto and L. Senatore, *Isocurvature constraints on gravitationally produced superheavy dark matter*, *Phys. Rev. D* **72** (2005) 023511 [[astro-ph/0411468](#)].
- [38] D. J. H. Chung and H. Yoo, *Isocurvature Perturbations and Non-Gaussianity of Gravitationally Produced Nonthermal Dark Matter*, *Phys. Rev. D* **87** (2013) 023516 [[1110.5931](#)].
- [39] D. J. H. Chung, H. Yoo and P. Zhou, *Quadratic Isocurvature Cross-Correlation, Ward Identity, and Dark Matter*, *Phys. Rev. D* **87** (2013) 123502 [[1303.6024](#)].
- [40] D. J. H. Chung and H. Yoo, *Elementary Theorems Regarding Blue Isocurvature Perturbations*, *Phys. Rev. D* **91** (2015) 083530 [[1501.05618](#)].
- [41] T. Markkanen, *Renormalization of the inflationary perturbations revisited*, *JCAP* **05** (2018) 001 [[1712.02372](#)].
- [42] N. Herring, D. Boyanovsky and A. R. Zentner, *Nonadiabatic cosmological production of ultralight dark matter*, *Phys. Rev. D* **101** (2020) 083516 [[1912.10859](#)].
- [43] M. A. G. Garcia, M. Pierre and S. Verner, *Isocurvature constraints on scalar dark matter production from the inflaton*, *Phys. Rev. D* **107** (2023) 123508 [[2303.07359](#)].
- [44] P. B. Greene and L. Kofman, *Preheating of fermions*, *Phys. Lett. B* **448** (1999) 6 [[hep-ph/9807339](#)].
- [45] Y. Ema, R. Jinno, K. Mukaida and K. Nakayama, *Gravitational Effects on Inflaton Decay*, *JCAP* **05** (2015) 038 [[1502.02475](#)].
- [46] M. Garny, M. Sandora and M. S. Sloth, *Planckian Interacting Massive Particles as Dark Matter*, *Phys. Rev. Lett.* **116** (2016) 101302 [[1511.03278](#)].

- [47] Y. Ema, R. Jinno, K. Mukaida and K. Nakayama, *Gravitational particle production in oscillating backgrounds and its cosmological implications*, *Phys. Rev. D* **94** (2016) 063517 [[1604.08898](#)].
- [48] Y. Tang and Y.-L. Wu, *On Thermal Gravitational Contribution to Particle Production and Dark Matter*, *Phys. Lett. B* **774** (2017) 676 [[1708.05138](#)].
- [49] M. Garny, A. Palessandro, M. Sandora and M. S. Sloth, *Theory and Phenomenology of Planckian Interacting Massive Particles as Dark Matter*, *JCAP* **02** (2018) 027 [[1709.09688](#)].
- [50] N. Bernal, M. Dutra, Y. Mambrini, K. Olive, M. Peloso and M. Pierre, *Spin-2 Portal Dark Matter*, *Phys. Rev. D* **97** (2018) 115020 [[1803.01866](#)].
- [51] Y. Ema, K. Nakayama and Y. Tang, *Production of Purely Gravitational Dark Matter*, *JHEP* **09** (2018) 135 [[1804.07471](#)].
- [52] M. Garny, A. Palessandro, M. Sandora and M. S. Sloth, *Charged Planckian Interacting Dark Matter*, *JCAP* **01** (2019) 021 [[1810.01428](#)].
- [53] T. Opferkuch, P. Schwaller and B. A. Stefanek, *Ricci Reheating*, *JCAP* **07** (2019) 016 [[1905.06823](#)].
- [54] M. Chianese, B. Fu and S. F. King, *Impact of Higgs portal on gravity-mediated production of superheavy dark matter*, *JCAP* **06** (2020) 019 [[2003.07366](#)].
- [55] N. Herring and D. Boyanovsky, *Gravitational production of nearly thermal fermionic dark matter*, *Phys. Rev. D* **101** (2020) 123522 [[2005.00391](#)].
- [56] Y. Mambrini and K. A. Olive, *Gravitational Production of Dark Matter during Reheating*, *Phys. Rev. D* **103** (2021) 115009 [[2102.06214](#)].
- [57] N. Bernal and C. S. Fong, *Dark matter and leptogenesis from gravitational production*, *JCAP* **06** (2021) 028 [[2103.06896](#)].
- [58] B. Barman and N. Bernal, *Gravitational SIMPs*, *JCAP* **06** (2021) 011 [[2104.10699](#)].
- [59] R. Garani, M. Redi and A. Tesi, *Dark QCD matters*, *JHEP* **12** (2021) 139 [[2105.03429](#)].
- [60] A. Ahmed, B. Grzadkowski and A. Socha, *Implications of time-dependent inflaton decay on reheating and dark matter production*, *Phys. Lett. B* **831** (2022) 137201 [[2111.06065](#)].
- [61] S. Clery, Y. Mambrini, K. A. Olive and S. Verner, *Gravitational portals in the early Universe*, *Phys. Rev. D* **105** (2022) 075005 [[2112.15214](#)].
- [62] M. R. Haque and D. Maity, *Gravitational dark matter: Free streaming and phase space distribution*, *Phys. Rev. D* **106** (2022) 023506 [[2112.14668](#)].
- [63] M. R. Haque and D. Maity, *Gravitational reheating*, *Phys. Rev. D* **107** (2023) 043531 [[2201.02348](#)].
- [64] S. Aoki, H. M. Lee, A. G. Menkara and K. Yamashita, *Reheating and dark matter freeze-in in the Higgs- R^2 inflation model*, *JHEP* **05** (2022) 121 [[2202.13063](#)].
- [65] S. Clery, Y. Mambrini, K. A. Olive, A. Shkerin and S. Verner, *Gravitational portals with nonminimal couplings*, *Phys. Rev. D* **105** (2022) 095042 [[2203.02004](#)].
- [66] A. Ahmed, B. Grzadkowski and A. Socha, *Higgs boson induced reheating and ultraviolet frozen-in dark matter*, *JHEP* **02** (2023) 196 [[2207.11218](#)].

- [67] M. A. G. Garcia, M. Pierre and S. Verner, *Scalar dark matter production from preheating and structure formation constraints*, *Phys. Rev. D* **107** (2023) 043530 [[2206.08940](#)].
- [68] E. Basso, D. J. H. Chung, E. W. Kolb and A. J. Long, *Quantum interference in gravitational particle production*, *JHEP* **12** (2022) 108 [[2209.01713](#)].
- [69] K. Kaneta, S. M. Lee and K.-y. Oda, *Boltzmann or Bogoliubov? Approaches compared in gravitational particle production*, *JCAP* **09** (2022) 018 [[2206.10929](#)].
- [70] B. Barman, S. Cléry, R. T. Co, Y. Mambrini and K. A. Olive, *Gravity as a portal to reheating, leptogenesis and dark matter*, *JHEP* **12** (2022) 072 [[2210.05716](#)].
- [71] M. R. Haque, D. Maity and R. Mondal, *WIMPs, FIMPs, and Inflaton phenomenology via reheating, CMB and ΔN_{eff}* , *JHEP* **09** (2023) 012 [[2301.01641](#)].
- [72] D. G. Figueroa, T. Opferkuch and B. A. Stefanek, *Ricci Reheating on the Lattice*, [2404.17654](#).
- [73] T. Markkanen and A. Rajantie, *Massive scalar field evolution in de Sitter*, *JHEP* **01** (2017) 133 [[1607.00334](#)].
- [74] L. Li, T. Nakama, C. M. Sou, Y. Wang and S. Zhou, *Gravitational Production of Superheavy Dark Matter and Associated Cosmological Signatures*, *JHEP* **07** (2019) 067 [[1903.08842](#)].
- [75] S. P. Corbà and L. Sorbo, *On adiabatic subtraction in an inflating Universe*, *JCAP* **07** (2023) 005 [[2209.14362](#)].
- [76] D. J. H. Chung, E. W. Kolb and A. J. Long, *Gravitational production of super-Hubble-mass particles: an analytic approach*, *JHEP* **01** (2019) 189 [[1812.00211](#)].
- [77] D. J. H. Chung, *Classical Inflation Field Induced Creation of Superheavy Dark Matter*, *Phys. Rev. D* **67** (2003) 083514 [[hep-ph/9809489](#)].
- [78] S. Enomoto, S. Iida, N. Maekawa and T. Matsuda, *Beauty is more attractive: particle production and moduli trapping with higher dimensional interaction*, *JHEP* **01** (2014) 141 [[1310.4751](#)].
- [79] S. Enomoto and T. Matsuda, *The exact WKB for cosmological particle production*, *JHEP* **03** (2021) 090 [[2010.14835](#)].
- [80] L. Li, S. Lu, Y. Wang and S. Zhou, *Cosmological Signatures of Superheavy Dark Matter*, *JHEP* **07** (2020) 231 [[2002.01131](#)].
- [81] S. Hashiba, S. Ling and A. J. Long, *An analytic evaluation of gravitational particle production of fermions via Stokes phenomenon*, *JHEP* **09** (2022) 216 [[2206.14204](#)].
- [82] L. F. Abbott and M. B. Wise, *Constraints on Generalized Inflationary Cosmologies*, *Nucl. Phys. B* **244** (1984) 541.
- [83] F. Lucchin and S. Matarrese, *Power Law Inflation*, *Phys. Rev. D* **32** (1985) 1316.
- [84] A. A. Starobinsky, *A New Type of Isotropic Cosmological Models Without Singularity*, *Phys. Lett. B* **91** (1980) 99.
- [85] Y. B. Zeldovich and A. A. Starobinsky, *Particle production and vacuum polarization in an anisotropic gravitational field*, *Zh. Eksp. Teor. Fiz.* **61** (1971) 2161.
- [86] L. Kofman, A. D. Linde and A. A. Starobinsky, *Towards the theory of reheating after inflation*, *Phys. Rev. D* **56** (1997) 3258 [[hep-ph/9704452](#)].

- [87] R. Dabrowski and G. V. Dunne, *Superadiabatic particle number in Schwinger and de Sitter particle production*, *Phys. Rev. D* **90** (2014) 025021 [[1405.0302](#)].
- [88] R. Dabrowski and G. V. Dunne, *Time dependence of adiabatic particle number*, *Phys. Rev. D* **94** (2016) 065005 [[1606.00902](#)].
- [89] P. R. Anderson and E. Mottola, *Instability of global de Sitter space to particle creation*, *Phys. Rev. D* **89** (2014) 104038 [[1310.0030](#)].
- [90] P. R. Anderson and E. Mottola, *Quantum vacuum instability of “eternal” de Sitter space*, *Phys. Rev. D* **89** (2014) 104039 [[1310.1963](#)].
- [91] J. Martin, C. Ringeval and V. Vennin, *Encyclopædia Inflationaris*, *Phys. Dark Univ.* **5-6** (2014) 75 [[1303.3787](#)].
- [92] S. Unnikrishnan and V. Sahni, *Resurrecting power law inflation in the light of Planck results*, *JCAP* **10** (2013) 063 [[1305.5260](#)].
- [93] R. Brandenberger, V. Kamali and R. O. Ramos, *Minimal Preheating*, [2305.11246](#).
- [94] G. F. Giudice, E. W. Kolb and A. Riotto, *Largest temperature of the radiation era and its cosmological implications*, *Phys. Rev. D* **64** (2001) 023508 [[hep-ph/0005123](#)].
- [95] M. A. G. Garcia, K. Kaneta, Y. Mambrini and K. A. Olive, *Reheating and Post-inflationary Production of Dark Matter*, *Phys. Rev. D* **101** (2020) 123507 [[2004.08404](#)].
- [96] C. Pallis, *Kination-dominated reheating and cold dark matter abundance*, *Nucl. Phys. B* **751** (2006) 129 [[hep-ph/0510234](#)].
- [97] BICEP, KECK collaboration, P. A. R. Ade et al., *Improved Constraints on Primordial Gravitational Waves using Planck, WMAP, and BICEP/Keck Observations through the 2018 Observing Season*, *Phys. Rev. Lett.* **127** (2021) 151301 [[2110.00483](#)].
- [98] WINDCHIME collaboration, A. Attanasio et al., *Snowmass 2021 White Paper: The Windchime Project*, in *Snowmass 2021*, 3, 2022, [2203.07242](#).
- [99] D. Carney, S. Ghosh, G. Krnjaic and J. M. Taylor, *Proposal for gravitational direct detection of dark matter*, *Phys. Rev. D* **102** (2020) 072003 [[1903.00492](#)].
- [100] J. Quintin, Y.-F. Cai and R. H. Brandenberger, *Matter creation in a nonsingular bouncing cosmology*, *Phys. Rev. D* **90** (2014) 063507 [[1406.6049](#)].
- [101] C. K. Dumlu and G. V. Dunne, *The Stokes Phenomenon and Schwinger Vacuum Pair Production in Time-Dependent Laser Pulses*, *Phys. Rev. Lett.* **104** (2010) 250402 [[1004.2509](#)].
- [102] M. V. Berry, *Uniform asymptotic smoothing of stokes’s discontinuities*, *Proceedings of the Royal Society of London. Series A, Mathematical and Physical Sciences* **422** (1989) 7.
- [103] M. V. Berry, *Waves near stokes lines*, *Proceedings of the Royal Society of London. Series A, Mathematical and Physical Sciences* **427** (1990) 265.